MIT Libraries | DSpace@MIT

MIT Open Access Articles

The discovery of y dwarfs using data from the wide-field infrared survey explorer (WISE)

Massachusetts Institute of Technology

THE DISCOVERY OF Y DWARFS USING DATA FROM THE WIDE-FIELD INFRARED SURVEY EXPLORER (WISE)

Michael C. Cushing[A], J. Davy Kirkpatrick[B], Christopher R. Gelino[B], Roger L. Griffith[B], Michael F. Skrutskie[C], Amanda K. Mainzer[D], Kenneth A. Marsh[B], Charles A. Beichman[B], Adam J. Burgasser[E,F], Lisa A. Prato[G], Robert A. Simcoe[F], Mark S. Marley[H], D. Saumon[I], Richard S. Freedman[H], Peter R. Eisenhardt[D], & Edward L. Wright[J]

Draft version August 24, 2011

ABSTRACT

We present the discovery of seven ultracool brown dwarfs identified with the Wide-field Infrared Survey Explorer (WISE). Near-infrared spectroscopy reveals deep absorption bands of H_2O and CH_4 that indicate all seven of the brown dwarfs have spectral types later than UGPS J072227.51−054031.2, the latest type T dwarf currently known. The spectrum of WISEP J182831.08+265037.8 is distinct in that the heights of the J- and H-band peaks are approximately equal in units of f_λ, so we identify it as the archetypal member of the Y spectral class. The spectra of at least two of the other brown dwarfs exhibit absorption on the blue wing of the H-band peak that we tentatively ascribe to NH_3. These spectral morphological changes provide a clear transition between the T dwarfs and the Y dwarfs. In order to produce a smooth near-infrared spectral sequence across the T/Y dwarf transition, we have reclassified UGPS 0722−05 as the T9 spectral standard and tentatively assign WISEP J173835.52+273258.9 as the Y0 spectral standard. In total, six of the seven new brown dwarfs are classified as Y dwarfs: four are classified as Y0, one is classified as Y0 (pec?), and WISEP J1828+2650 is classified as >Y0. We have also compared the spectra to the model atmospheres of Marley and Saumon and infer that the brown dwarfs have effective temperatures ranging from 300 K to 500 K, making them the coldest spectroscopically confirmed brown dwarfs known to date.

Subject headings: infrared: stars — stars: low-mass, brown dwarfs — stars: individual (UGPS J072227.51−054031.2, WISEPC J014807.25−720258.8, WISEP J041022.71+150248.5, WISEPC J140518.40+553421.5, WISEP J154151.65−225025.2, WISEP J173835.52+273258.9, WISEP J1828+2650, WISEPC J205628.90+145953.3)

1. INTRODUCTION

Brown dwarfs, objects with too little mass to sustain the high core temperatures necessary for stable thermonuclear fusion of hydrogen, are the least massive, and possibly the most numerous products of star formation. Although first predicted to exist in the early 1960's (Kumar 1963; Hayashi & Nakano 1963), it was not until decades later that brown dwarfs were discovered in bulk by wide-area, red (700−1000 nm) and near-infrared (1−2.5 μm) capable surveys such as the Two Micron All Sky Survey (2MASS, Skrutskie et al. 2006), the Sloan Digital Sky Survey (SDSS, York et al. 2000) and the Deep Near-Infrared Southern Sky Survey (DE-NIS, Epchtein et al. 1997). The emergent spectra of brown dwarfs are so distinct from that of late-type M dwarfs that the creation of two new spectral classes, L and T (Kirkpatrick et al. 1999; Burgasser et al. 2006), was required in order to properly classify them[11]. The latest type T dwarfs currently known were discovered in the UKIRT Infrared Deep Sky Survey (UKIDSS, Lawrence et al. 2007) and the Canada France Brown Dwarf Survey (CFBDS, Delorme et al. 2008b) and have estimated effective temperatures (T_{eff}s) of 500 to 700 K (e.g., Burningham et al. 2008; Delorme et al. 2008a; Leggett et al. 2009; Lucas et al. 2010; Liu et al. 2011).

Despite these spectacular successes, there exists a gap of nearly 400 K between the coolest spectroscopically confirmed brown dwarfs at $T_{eff} \sim 500$ K (Lucas et al. 2010) and Jupiter at $T_{eff} \sim 124$ K (Hanel et al. 1981). Although observations of star formation regions and young associations such as the Orion Nebula Cluster (Weights et al. 2009), Chameleon I (Luhman et al. 2005), and TW Hydrae (Chauvin et al. 2004) suggest that nature can form brown dwarfs that will eventually cool to these temperatures once they have dispersed from their natal clusters, they are simply too faint to

[a] Jet Propulsion Laboratory, California Institute of Technology 4800 Oak Grove Drive, MS 321-520, Pasadena, CA 91109; michael.cushing@gmail.com
[b] Infrared Processing and Analysis Center, California Institute of Technology, Pasadena, CA 91125
[c] Department of Astronomy, University of Virginia, Charlottesville, VA, 22904
[d] Jet Propulsion Laboratory, California Institute of Technology 4800 Oak Grove Drive, Pasadena, CA 91109
[e] Center for Astrophysics and Space Science, University of California San Diego, La Jolla, CA 92093, Hellman Fellow
[f] Massachusetts Institute of Technology, 77 Massachusetts Avenue, Building 37, Cambridge, MA 02139
[g] Lowell Observatory, 1400 West Mars Hill Road, Flagstaff, AZ, 86001
[h] NASA Ames Research Center, MS 254-3, Moffett Field, CA 94035
[i] Los Alamos National Laboratory, MS F663, Los Alamos, NM 87545
[j] Department of Physics and Astronomy, UCLA, Los Angeles, CA 90095

[11] A compendium of known L and T dwarfs can be found at http://DwarfArchives.org

have been detected by the aforementioned surveys. Recently however, two brown dwarfs with estimated effective temperatures of $300-400$ K, WD $0806-661$B (Luhman et al. 2011) and CFBDSIR J145829+101343B (CFBDSIR J1458+1013B Liu et al. 2011), were discovered in targeted searches for companions to nearby stars. Although efforts to obtain spectra of these two common proper motion sources have been hampered by extreme faintness in the case of WD $0806-661$($J > 21.7$; Rodriguez et al. 2011), and proximity to its primary star in the case of CFBDSIR J1458+1013B ($<0.''1$), their mere existence suggests that a population of nearby cold brown dwarfs awaits discovery.

Foremost is the question of what these objects will look like spectroscopically and whether a new spectral class beyond T, dubbed "Y" (Kirkpatrick et al. 1999; Kirkpatrick 2000), will be required in order to properly classify them. Chemical equilibrium calculations and model atmospheres predict that as brown dwarfs cool below $T_{\rm eff} \sim 600$ K, their atmospheres pass through a series of chemical transitions which in turn impact the appearance of their emergent spectra (Lodders 1999; Burrows & Sharp 1999; Lodders & Fegley 2002; Burrows et al. 2003). At $T_{\rm eff} \sim 600$ K, the combination and overtone bands of NH_3 emerge in the near-infrared[12]. At $T_{\rm eff} \sim 500$ K, the prominent resonance absorption lines of Na I and K I in the red optical spectra of warmer brown dwarfs weaken as Na condenses out of the gas phase into Na_2S and then K condenses into KCl. Finally, H_2O and NH_3 will also condense out at $T_{\rm eff} \sim 350$ K and ~ 200 K, respectively. Although each transition has been suggested as the trigger for the Y spectral class, focus has primarily been on detecting the NH_3 bands because they are predicted to emerge at the hottest effective temperatures. Although NH_3 absorption has been tentatively detected in the near-infrared spectrum of CFBDS J005910.90$-$011401.3 (hereafter CFBDS J0059$-$0114, Delorme et al. 2008a), this feature has not been confirmed in the spectrum of the cooler object UGPS J072227.51$-$054031.2 (UGPS 0722$-$05; Lucas et al. 2010).

Independent of their spectral morphology, the study of these ultracool brown dwarfs will provide important insights into both ultracool atmospheric physics and the low-mass end of the stellar mass function. Because brown dwarfs and exoplanets have similar atmospheric conditions, ultracool brown dwarfs are also excellent exoplanet analogs that can be used as benchmarks for model atmospheres. The study of these ultracool brown dwarfs will therefore directly inform the interpretation and characterization of exoplanets detected with the next generation of high-contrast imagers like the Gemini Planet Imager (GPI; Macintosh et al. 2006) the Spectro-Polarimetric High-contrast Exoplanet Research instrument for the VLT (SPHERE; Beuzit et al. 2006), Project 1640 at Palomar Observatory (Hinkley et al. 2011), and the L- and M-band Infrared Camera (LMIRcam; Skrutskie et al. 2010) for the Large Binocular Telescope Interferometer (LBTI). Simulations by Burgasser

---

[12] Although the fundamental band of NH_3 has been detected in the spectra of warmer T dwarfs at 10.5 μm (e.g., Roellig et al. 2004; Cushing et al. 2006), the intrinsically weaker near-infrared bands require a higher NH_3 abundance, and thus lower effective temperature, to become a dominant opacity source.

(2004) and Allen et al. (2005) have also shown that the space density of cold brown dwarfs is very sensitive to both the underlying mass function and the low-mass limit of star formation. Identifying and characterizing a statistically robust sample of cold brown dwarfs will therefore provide two critical constraints on theories of low-mass star formation (Whitworth & Stamatellos 2006; Whitworth et al. 2007).

One of the primary science goals of the Wide-field Infrared Survey Explorer (WISE, Wright et al. 2010), a NASA mission that recently surveyed the entire sky at 3.4 (W1), 4.6 (W2), 12 (W3), and 22 (W4) μm, is to identify such cold brown dwarfs. The W1 and W2 bands were designed specifically to sample the deep CH_4 absorption band centered at 3.3 μm and the region relatively free of opacity centered at ~ 4.7 μm in the spectra of cold brown dwarfs (see Figure 2 of Mainzer et al. 2011). Since the peak of the Planck function at these low effective temperatures is in the mid-infrared, a large amount of flux emerges from the 4.7 μm opacity hole, making the W1$-$W2 colors extremely red (W1$-$W2 > 2, Mainzer et al. 2011; Kirkpatrick et al. 2011). Indeed such red colors are almost unique amongst astronomical sources making the identification of cool brown dwarfs with the W1$-$W2 color alone relatively easy (see Figure 12 of Wright et al. 2010).

We have been conducting a search for cold brown dwarfs since the start of the WISE survey in mid January 2010. This search has already born fruit with the discovery of six late-type T dwarfs (Mainzer et al. 2011; Burgasser et al. 2011) two of which have spectral types later than T8. Kirkpatrick et al. (2011) present over 100 new brown dwarfs, the vast majority of which have spectral types later than T6. In this paper, we focus on seven of the ~ 100 brown dwarfs whose near-infrared spectra indicate that the they are the latest-type spectroscopically confirmed brown dwarfs currently known. Indeed we identify six of these brown dwarfs as the first members of the Y spectral class. In §2, we briefly discuss our selection criteria before presenting the ground- and spaced-based imaging and spectroscopic followup observations in §3. In §4 we present the properties of the first Y dwarfs, define the transition between the T sequence and the Y dwarfs, and derive estimates of the atmospheric parameters of the new brown dwarfs using model atmospheres.

2. CANDIDATE SELECTION

The seven new brown dwarfs were identified as part of a larger ongoing search for cold brown dwarfs using WISE. A detailed description of this survey and our search criteria is presented by Kirkpatrick et al. (2011). Briefly, candidates were selected from the source working database derived from the first-pass processing operational coadds using color constraints derived from known T dwarfs and model atmospheres (in the case of brown dwarfs with $T_{\rm eff}$ < 500 K). Table 1 lists the WISE designations and photometry of the seven brown dwarfs, and Figure 1 shows 2$'$ x 2$'$ DSS I, 2MASS J and H, WISE W1, W2, and W3, and W1W2W3 color composite images for each dwarf. Hereafter we abbreviate the numerical portions of the WISE designations as hhmm±ddmm, where the suffix is the sexagesimal right ascension (hours and minutes) and declination (degrees and arcminutes) at J2000.0 equinox.

3. OBSERVATIONS

The followup ground- and space-based observations of the seven WISE brown dwarfs are discussed in the following sections. Although we present the near-infrared photometry of the brown dwarfs in this work for completeness, we defer the discussion of these data to Kirkpatrick et al. (2011) who present a more detailed discussion that places them in context with the larger population of brown dwarfs. In addition to the observations of the seven WISE brown dwarfs, we also obtained a near-infrared spectrum of UGPS 0722−05 for comparison purposes. A log of the near-infrared photometric observations as well as the resulting photometry is given in Table 2, and a log of the spectroscopic observations is given in Table 3.

3.1. Near-Infrared Imaging
3.1.1. NEWFIRM/Blanco

WISEP J1541−2250 was observed on the night of 2011 Apr 17 (UT) with the NOAO Extremely Wide Field Infrared Imager (NEWFIRM) mounted on the Cerro Tololo Inter-American Observatory (CTIO) Victor M. Blanco 4m Telescope. A description of the instrument, observing strategy, and data reduction can be found in Kirkpatrick et al. (2011). The resultant J- and H-band photometry is presented in Table 2.

3.1.2. WIRC/Palomar

Near-infrared images of WISEP J0410+1502, WISEPC J1405+5534, WISEP J1738+2732, and WISEPC J2056+1459 were obtained using the Wide-field Infrared Camera (WIRC; Wilson et al. 2003) on the 200 inch Hale Telescope at Palomar Observatory. A description of the instrument, observing strategy, and data reduction can be found in Kirkpatrick et al. (2011). The magnitudes and/or limits for each brown dwarf are given in Table 2.

3.1.3. PANIC/Magellan

WISEPC J0148−7202 was observed on the night of 2010 Aug 01 (UT) with the now decommissioned Persson's Auxiliary Nasmyth Infrared Camera (PANIC; Martini et al. 2004) on the east Nasmyth platform at the Magellan 6.5 m Baade Telescope. A description of the instrument, observing strategy, and data reduction can be found in Kirkpatrick et al. (2011). The J- and H-band magnitudes of WISEPC J0148−7202 are given in Table 2.

3.1.4. NIRC2/Keck II

High resolution observations of WISEP J1828+2650 and WISEPC J2056+1459 were obtained with NIRC2 behind the Keck II LGS-AO system (Wizinowich et al. 2006; van Dam et al. 2006) on the night of 2010 July 1 (UT). A description of the instrument, observing strategy, and data reduction can be found in Kirkpatrick et al. (2011). The J- and H-band magnitudes are given in Table 2.

3.2. Near-Infrared Spectroscopy
3.2.1. SpeX/IRTF

A 0.9−2.5 μm, low-resolution ($R \equiv \lambda/\Delta\lambda \approx 150$) spectrum of UGPS 0722−05 was obtained with SpeX (Rayner et al. 2003) on the 3 m NASA IRTF on 26 Jan 2011 (UT). A description of the instrument, observing strategy, and data reduction can be found in Kirkpatrick et al. (2011). The spectrum, which is shown in Figure 2, has a high S/N, reaching >50 at the peaks of the Y, J, and H bands.

3.2.2. FIRE/Magellan

Low-resolution (R=250−350), 1−2.4 μm spectra of WISEPC J0148−7202, WISEP J0410+1502, and WISEP J1541−2250 were obtained with the Folded-port InfraRed Echellette (FIRE, Simcoe et al. 2008, 2010) mounted at the auxiliary Nasmyth focus of the Magellan 6.5 m Baade Telescope . A description of the instrument, observing strategy, and data reduction can be found in Kirkpatrick et al. (2011). The spectra are shown in Figure 2.

3.2.3. NIRSPEC/Keck II

WISEPC J2056+1459 was observed using the Near-Infrared Spectrometer (NIRSPEC; McLean et al. 1998, 2000) located on one of the Nasmyth platforms of the 10 m Keck II telescope on Mauna Kea, Hawai'i. The 0.″38-wide slit in the low resolution mode provides a resolving power of R=2500. WISEPC J2056+1459 was observed with the N3 order sorting filter (1.143−1.375 μm) on the night of 2010 Oct 21 (UT) and with the N5 order sorting filter (1.431−1.808 μm) on the night of 2010 Nov 22 (UT).

A series of 300 s exposures was obtained at two different positions along the 42″ long slit. An A0 V star was observed after each series of science exposures for telluric correction and flux calibration purposes. Calibration frames consisting of neon and argon arc lamps, dark frames, and flat-field lamps were also taken following the science exposures. The data were reduced in a standard fashion using the IDL-based REDSPEC[13] reduction package as described in McLean et al. (2003). Since REDSPEC does not produce uncertainty arrays, we generated them as follows. First we performed a simple sum extraction using the rectified, pair-subtracted images generated by REDSPEC. We then scaled the spectra to a common flux level and computed the average spectrum. The uncertainty at each wavelength is given by the standard error on the mean. The average spectrum is then corrected for telluric absorption and flux calibrated using the calibration spectrum generated by REDSPEC. Since the difference between the spectra produced by REDSPEC and our spectra was negligible, we used our spectrum for our analysis. Finally, the N3− and N5−band spectra were absolutely flux calibrated using the WIRC photometry (see Table 2) as described in Cushing et al. (2005) and merged to produce a 1.15−1.80 μm spectrum. The final spectrum, which is shown in Figure 2, has a peak S/N of 8 and 6 in the J and H bands, respectively.

3.2.4. WFC3/Hubble Space Telescope

---

[13] See http://www2.keck.hawaii.edu/inst/nirspec/redspec.

WISEPC J1405+5534, WISEP J1738+2732, and WISEP J1828+2650 were observed with the infrared channel of the Wide Field Camera 3 (WFC3; Kimble et al. 2008) on-board the *Hubble Space Telescope* (HST) as a part of a Cycle 18 program (GO-12330, PI=Kirkpatrick). The WFC3 uses a 1024×1024 HgCdTe detector with a plate scale of $0''13$ pixel^{-1} which results in a field of view of 123×126 arcsecond. The G141 grism was used to perform slitless spectroscopy of each brown dwarf covering the $1.07-1.70$ μm wavelength range at a resolving power of $R \approx 130$. For each brown dwarf, we first obtained four direct images through the F140W filter (λ_p=1392.3 nm) in the MULTIACCUM mode with the SPARS25 sampling sequence. Between each exposure the telescope was offset slightly. We then obtained four images with the G141 grism at the same positions as the direct images. The spectroscopic observations were also obtained in the MUTLIACCUM mode but using the SPARS50 sequence.

The raw images were first processed using the CAL-WFC3 pipeline (version 2.3) which not only subtracts the bias level and dark current but also flat fields the direct images (the grism images are flat fielded during the extraction process described below). The spectra were then extracted using the aXe software (Kümmel et al. 2009), which is a suite of PyRAF/IRAF packages designed to extract spectra from the slitless modes of both WFC3 and the Advanced Camera for Surveys (ACS). aXe requires knowledge of both the position and brightness of the objects in the field of view. We therefore combined the four direct images using MULTIDRIZZLE (Koekemoer et al. 2002) and the latest Instrument Distortion Coefficient Table (IDCTAB). A catalog of the objects in the field was then constructed using SExtractor (Bertin & Arnouts 1996). For each object in the source catalog, two dimensional (2D) subimages centered on the first-order spectra of each object were then combined using the task AXEDRIZZLE to produce a high S/N 2D spectral image. One-dimensional, flux-calibrated spectra and their associated uncertainties are then extracted from the 2D drizzle subimages.

Since the G141 grism mode is slitless, spectral contamination from nearby sources is not uncommon. The aXe software (using the Gaussian emission model) estimates the level of contamination for each object using the positions and magnitudes of all the objects in the field of view. The spectrum of one of the brown dwarfs, WISEP J1828+2650, exhibits moderate contamination that increases in intensity towards shorter wavelengths (see Figure 3). The aXe software does not actually correct for this contamination so we attempted to do so using the contamination image generated by aXe. Unfortunately, the contamination-corrected spectrum exhibits negative flux values which suggests that aXe is over estimating the contamination level. We will therefore use the contaminated spectrum and consider it an upper limit to the actual spectrum. This issue will be discussed in more detail in §4.1.1.

4. ANALYSIS

4.1. *Spectral Characterization*

Figure 2 shows the near-infrared spectra of the new brown dwarfs. Also plotted for comparison purposes is our IRTF/SpeX spectrum of UGPS 0722$-$05, the latest type brown dwarf known previous to this work. All of the spectra exhibit deep H_2O and CH_4 absorption bands characteristic of late-type T dwarfs but the J-band peaks of the WISE brown dwarfs are narrower than the corresponding peak in the spectrum of UGPS 0722$-$05. This peak becomes progressively narrower beyond T8 (Warren et al. 2007; Delorme et al. 2008a; Burningham et al. 2008; Lucas et al. 2010), indicating that all of the WISE brown dwarfs have spectral types later than UGPS 0722$-$05. The spectrum of WISEP J1828+2650 is markedly different than that of UGPS 0722$-$05 so we discuss this object in more detail in the following section before discussing the other six dwarfs.

4.1.1. *WISEP J1828+2650: The Archetypal Y Dwarf*

The lower panel of Figure 4 shows the $1.15-1.70$ μm spectrum of WISEP J1828+2650 along with the spectrum of UGPS 0722$-$05. The spectrum of WISEP J1828+2650, while dominated by the same CH_4 and H_2O absorption bands present in T dwarf spectra, has a feature not seen in any T dwarf: the J- and H-band peaks, when plotted in units of f_λ, are essentially the same height. As discussed in §3.2.4, the spectrum of WISEP J1828+2650 is contaminated by light from nearby stars. This contamination, which is *not* removed by the aXe software, becomes progressively worse at shorter wavelengths (see Figure 3) such that the true spectrum will have an even more extreme J to H band peak flux ratio.

The roughly equal-intensity J and H flux peaks are also confirmed by our ground-based, near-infrared photometry, which gives $J - H = 0.72 \pm 0.42$ mag. Model atmospheres of cool brown dwarfs predict that the near-infrared colors, which are blue for the hotter T dwarfs, turn back to the red at effective temperatures between 300 and 400 K as the Wien tail of the spectral energy distribution collapses. This turn to the red was proposed as one of the triggers that might force the creation of a Y spectral class (Burrows et al. 2003; Kirkpatrick 2008).

Further underscoring the extreme nature of WISEP J1828+2650 is its $J-W2$ color of 9.29 ± 0.35 which is over 2 mags redder than the WISEP J1541$-$2250, the second reddest brown dwarf in our sample at $J-W2=7.18\pm0.38$ (Kirkpatrick et al. 2011). WISEP J1828+2650 is also the reddest brown dwarf in our sample in $H-W2$, $J-[4.5]$, and $H-[4.5]$, where [4.5] represents the *Spitzer Space Telescope* (Werner et al. 2004) Infrared Array Camera (IRAC; Fazio et al. 2004) channel 2 magnitude. Given the extreme nature of both its near-infrared spectrum and near- to mid-infrared colors, we identify WISEP J1828+2650 as the archetypal member of the Y spectral class.

4.1.2. *WISEP J1738+2732 & WISEPC J1405+5534 and the 1.5 μm NH$_3$ Band*

The $1.15-1.70$ μm spectra of WISEPC J1405+5534 and WISEP J1738+2732 are very similar and yet both are distinct from UGPS 0722$-$05, albeit in less extreme

ways than the spectrum of WISEP J1828+2650 (see middle and upper panels of Figure 4). Although the relative heights of the J- and H-band peaks are similar to those of UGPS 0722−05, their widths are narrower. The narrowing of the H-band peaks is asymmetric, however, as most of the change is a result of enhanced absorption on the blue wings from 1.51−1.58 μm. What is the underlying cause of this absorption?

The H-band spectra of T dwarfs are shaped by CH_4 (and to a lesser extent H_2O) longward of 1.6 μm and by H_2O at wavelengths shortward of 1.6 μm. As the effective temperature falls, the opacity of the near infrared overtone and combination bands of NH_3 becomes important since $NH_3/N_2 > 1$ for $T \lesssim 700$ K at P=1 bar (Lodders & Fegley 2002). The emergence of these NH_3 bands has long been suggested as the trigger for a new spectral class (Burrows et al. 2003; Kirkpatrick 2008; Leggett et al. 2007a) but identifying them has proven difficult because they overlap with the strong H_2O bands and because the abundance of NH_3 can be reduced by an order of magnitude due to vertical mixing in the atmospheres of brown dwarfs (Saumon et al. 2003, 2006; Hubeny & Burrows 2007).

Figure 5 shows the H-band spectra of the T4, T6, and T8 spectral standards, UGPS 0722−05, and WISEP J1738+2732 as well as the opacities for H_2O (Freedman et al. 2008), NH_3 (Yurchenko et al. 2011), and CH_4 (Freedman et al. 2008) at T=600 K and P=1 bar generated by one of us by (R.S.F.). With increasing spectral type, the blue-wing of the H-band peak becomes progressively suppressed. Delorme et al. (2008a) tentatively identified NH_3 absorption on the blue wing of the H-band spectrum of CFBDS J0059−0114, a T dwarf with a spectral type earlier than UGPS 0722−05. However, the change in the shape of the blue wing of the H-band peak from T6 to UGPS 0722−05 appears smooth, suggesting a common absorber or set of absorbers. It seems unlikely that NH_3 dominates given that it has not been identified in the spectra of mid-type T dwarf ($T_{\rm eff} \sim 1200$ K). A similar conclusion to ours is reached by Burningham et al. (2010) using spectral indices.

In contrast, the H-band spectrum of WISEP J1738+2732 stands out in the sequence in that it exhibits additional absorption from 1.53 to 1.58 μm. This absorption broadly matches the position of the $\nu_1 + \nu_3$ absorption band of NH_3 centered at 1.49 μm suggesting that NH_3 is the cause of this absorption. However, we cannot conclusively identify NH_3 as the carrier given the low spectral resolution of the data and the fact that the absorption lies on the steep wing of the H_2O band. For example, water ice also has an absorption band centered at $\sim$1.5 μm (Warren & Brandt 2008) that could potentially produce such absorption if the abundance of water ice is high enough. One potential avenue for confirming that NH_3 is indeed the carrier would be to acquire higher spectral resolution data to search for individual NH_3 features (e.g., Saumon et al. 2000; Warren et al. 2007).

4.1.3. The T Dwarf/Y Dwarf Transition

With WISEP J1828+2650 classified as the prototypical Y dwarf, we can now investigate the transition between the T and Y spectral classes. T dwarfs are classified at near-infrared wavelengths using the Burgasser et al. (2006) scheme, wherein nine T dwarf spectral standards with subtypes ranging from T0 to T8 are used for direct spectral comparisons. Burgasser et al. also defined five spectral indices that measure the depths of the CH_4 and H_2O bands which can be used as a proxy for direct comparisons. With the discovery of brown dwarfs with spectral types later than T8, the question of how to extend the Burgasser et al. scheme beyond T8 naturally arises.

The first >T8 dwarf to be identified was ULAS J003402.77−005206.7 (ULAS J0034−0052; Warren et al. 2007). Based on a direct comparison to the spectrum of the T8 spectral standard and the values of the Burgasser et al. spectral indices, Warren et al. adopted a spectral type of T8.5. A second >T8 dwarf soon followed with the discovery of CFBDS J0059−0114 by Delorme et al. (2008a). They used the W_J index which measures the half-width of the J band peak (Warren et al. 2007) and the NH_3-H index which measures the half-width of the H-band peak (i.e. the depth of the putative NH_3 absorption), to classify both CFBDS J0059−0114 and ULAS J0034−0052 as T9 dwarfs. Burningham et al. (2008) added two T dwarfs to the tally of >T8 dwarfs with the discovery of ULAS J133553.45+113005.2 (ULAS J1335+1130) and ULAS J123828.51+095351.3 (ULAS J1238+0953). Using both direct spectral comparison and spectral indices, they classified them as T8.5 and T9, respectively. Burningham et al. also proposed extending the Burgasser et al. scheme to T9 by assigning ULAS J1335+1130 as the T9 spectral standard. Additional T dwarfs with spectral types later than T8 have since been discovered (see Table 5), but to date, the latest-type T dwarf currently known is UGPS 0722−05 (Lucas et al. 2010) which has been classified as T10 via a combination of spectral indices and direct comparisons to the T9 dwarfs.

Figure 6 shows the 1.15−1.70 μm spectra of the T6, T7, T8 spectral standards, UGPS 0722−05, and WISEP J1738+2732. The spectra show smooth changes in their spectral morphology with increasing spectral type including progressively deeper absorption bands centered at 1.15, 1.45, and 1.65 μm and progressively narrower J- and H-band peaks. However UGPS 0722−05 does not appear to be two subtypes later than T8 as required by its T10 spectral type. Rather, the changes in spectral morphology from T6 to UGPS 0722−05 suggest that UGPS 0722−05 is more naturally classified as a T9. Given its brightness (J=16.5, 1.5 mag brighter than ULAS J1335+1130) and position near the celestial equator, UGPS 0722−05 also makes an ideal spectral standard. We therefore define it to be the T9 spectral standard.

WISEP J1738+2732 is clearly of later type than UGPS 0722−05 but should it be classified as a T dwarf or a Y dwarf? As noted in the previous section, WISEP J1738+2732 exhibits excess absorption from 1.53 to 1.58 μm that we have tentatively ascribed to NH_3. This absorption becomes even more apparent when the spectrum is placed in sequence with the T6 to T9 spectral standards (lower right panel of Figure 6). Given the smooth change in width of the J-band peak and the rapid fall in the flux of the blue wing of the H-band between UGPS 0722−05 and WISEP J1738+2732 (which

suggests the emergence of a new absorption band), we classify WISEP J1738+2732 as a Y dwarf and assign it a spectral type of Y0. Additionally, we tentatively identify it as Y0 spectral standard.

4.1.4. *Classification of the Other WISE Discoveries*

With the T9 and Y0 spectral standards defined, we can return to the question of classifying the other new WISE discoveries. The J- and H-band peaks of WISEPC J0148−7202 are slightly narrower than UGPS 0722−05 and slightly wider than WISEP J1738+2732 so we classify this dwarf as T9.5. The spectrum of WISEPC J1405+5534 is very similar to that of WISEP J1738+2732 (see Figure 4). However, we note that the wavelength at which the peak H-band flux is reached is shifted ∼60 Å to the red relative to UGPS 0722−05 (see Figure 4) and the other late-type T dwarfs which suggests that WISEPC J1405+5534 may be peculiar. We therefore classify it as Y0 (pec?). Interestingly, a similar, albeit larger, shift of 200 Å is seen in the spectrum of Jupiter.

The spectra of the remaining brown dwarfs, WISEPC J2056+1459, WISEP J0410+1502, and WISEP J1541−2250, do not have sufficient S/N to convincingly show the excess absorption from 1.53−1.58 μm. However, the J-band peaks of these three brown dwarfs are all narrower than UGPS 0722−05. Indeed the spectra of all of them are a better match to the spectral morphology of WISEP J1738+2732 than UGPS 0722−05 so we classify these brown dwarfs as Y0 as well. In addition, the peak Y-band fluxes of WISEP J0410+1502 and WISEP J1541−2250 are slightly higher than in the spectrum of UGPS 0722−05. This is consistent with the blueward trend in the $Y - J$ color of late-type T dwarfs (Leggett et al. 2010; Burningham et al. 2010) which Burningham et al. (2010) ascribed to the weakening of the strong resonance K I doublet (7665, 7699 Å) as K condenses into KCl. Finally, since the spectrum of WISEP J1828+2650 is distinct from both UGPS 0722−05 and WISEP J1738+2732, we classify it as >Y0. A more precise subtype will require the discovery of additional Y dwarfs to bridge the gap in spectral morphology between WISEP J1738+2732 and WISEP J1828+2650.

4.1.5. *Reclassification of Previously Published ≥T8.5 Dwarfs*

There are also twelve T dwarfs with spectral types later than T8 currently in the literature (see Table 5). Since we have reclassified UGPS 0722−05 as a T9 dwarf, we must also reclassify the other eleven dwarfs using this new system. To accomplish this, we have smoothed the published spectra to a resolving power of R=150 and resampled them onto the same wavelength scale as the IRTF/SpeX spectrum of UGPS 0722−05. This ensures that differences in resolving power and wavelength sampling between the late-type T dwarfs and the Burgasser et al. IRTF/SpeX spectra of the T dwarf spectral standards do not adversely affect our classification. Table 5 gives the revised spectral types derived from direct comparison for the twelve T dwarfs with published spectral types later than T8. When the J and H band regions gave conflicting spectral types, we used the typed inferred from the J-band.

4.1.6. *Spectral Indices*

Although the primary (and preferred) method of assigning a spectral type is to compare the spectrum of a brown dwarf against that of the spectral standards, the use of spectral indices remains popular in the literature. We have therefore computed the H_2O-J, CH_4-J, H_2O-H, CH_4-H (Burgasser et al. 2006), W_J (Warren et al. 2007), and NH_3-H (Delorme et al. 2008a) indices of the new WISE brown dwarfs and as well as UGPS 0722−05. Figure 7 illustrates the positions of the indices' flux windows relative to the spectrum of UGPS 0722−05. The index values are computed in a Monte Carlo fashion whereby 5000 realizations of each spectrum are generated by randomly drawing from normal distributions with means given by the flux densities at each wavelength and standard deviations given by the uncertainty in the flux densities. The values of the indices and their uncertainties are given by the mean and standard deviation of the distribution of index values computed from the 5000 realizations and are listed in Table 4.

Figure 8 shows the values of the six indices as a function of spectral type. Also shown are the index values of the T6−T8 spectral standards, a sample of T5−T8 dwarfs from the SpeX Prism Spectral Library, and the twelve T dwarfs with previously published spectral types later than T8. The classification of WISEP J1738+2732 as a Y dwarf is bolstered by the distinctive break in the trend of the NH_3-H values with spectral type which suggests that a new absorption band has indeed emerged at the T/Y dwarf transition. The remaining spectral indices do not show a break at the T/Y transition, but the CH_4-J, H_2O-H, and W_J indices do show a smooth trend with spectral type down to Y0 indicating that they can still be used as proxies for direct spectral comparisons. Indeed the value of the W_J spectral index for WISEP J1738+2732 is far from saturated so we support the suggestion by Burningham et al. (2008) that this index can be used as a proxy for direct comparison for late-type T dwarfs and early-type Y dwarfs. However, the CH_4-H index is clearly beginning to saturate at T9 and the H_2O-J index may even reverse at Y0 rendering these indices less useful for classification purposes. Finally, although there is scatter due to the very low S/N of some of the spectra, the new WISE brown dwarfs are clearly distinct from the previous ≥T8.5 dwarfs and cluster around the Y0 spectral standard.

4.2. *Atmospheric and Structural Properties*
4.2.1. *Atmospheric Properties*

In order to investigate the atmospheric properties (e.g., $T_{\rm eff}$, $\log g$) of the brown dwarfs, we have compared their near-infrared spectra to a new preliminary grid of model spectra generated with the model atmospheres of Marley & Saumon. A detailed description of the basic models can be found in Marley et al. (2002), Saumon & Marley (2008), Cushing et al. (2008), and Stephens et al. (2009). This preliminary grid includes a new NH_3 line list (Yurchenko et al. 2011) and a new prescription for the collision induced opacity for H_2 (Saumon et al., in prep). A more detailed study that compares the model spectra to the near-infrared spectra, and WISE and *Spitzer* photometry is in preparation.

The grid consists of solar metallicity, cloudless mod-

els with the following parameters: $T_{\text{eff}}=200-1000$ K in steps of 50 K; $\log g = 3.75-5$ in steps of 0.25 (cm s^{-2}); and $K_{\text{zz}}=0$, 10^4 cm^2 s^{-1}. Although the opacities of the condensate clouds are not included in the atmospheric models, i.e. they are cloudless, the effects on the atmospheric chemistry due to the rainout of the condensates is accounted for in the models. This assumption is reasonable for the silicate and liquid iron clouds since they form well below the observable photosphere (see however, Burgasser et al. 2010) but may not be valid if, as expected, H$_2$O clouds form high in the atmosphere of the coldest models. The eddy diffusion coefficient, K_{zz}, parametrizes the vigor of mixing in the radiative layers of the atmosphere. A value of $K_{\text{zz}}>0$ cm^2 s^{-1} results in mixing that can prevent the abundances of CO and CH$_4$ (the dominant carbon-bearing species) from coming into chemical equilibrium because the mixing time scales become shorter than the timescales of key chemical reactions involved in the conversion of CO to CH$_4$ (Lodders & Fegley 2002; Saumon et al. 2003; Hubeny & Burrows 2007). Typical values of K_{zz} in the stratospheres of giant planets are 10^2 to 10^5 cm^2 s^{-1} (Saumon et al. 2006). The abundances of N$_2$ and NH$_3$ (the dominant nitrogen-bearing species) are also kept from coming into chemical equilibrium by mixing, but in this case the mixing timescales are set in the convective layers of the atmosphere by the mixing length theory. As a result, the final non-equilibrium abundances of N$_2$ and NH$_3$ are not sensitive to variations in the eddy diffusion coefficient K_{zz}. However by convention, models with $K_{\text{zz}}=0$ cm^2 s^{-1} are in full chemical equilibrium (i.e. the effect of convective mixing on the nitrogen chemistry is ignored) and models with $K_{\text{zz}}\neq 0$ cm^2 s^{-1} exhibit both carbon and nitrogen non-equilibrium chemistry.

The best fitting models are identified using the goodness-of-fit statistic, $G_k = \sum_{i=1}^{n} w_i \left(\frac{f_i - C_k \mathcal{F}_{k,i}}{\sigma_i} \right)^2$, where n is the number of data pixels; w_i is the weight for the ith wavelength (set to unity in this case); f_i and $F_{k,i}$ are the flux densities of the data and model k, respectively; σ_i are the errors in the observed flux densities; and C_k is an unknown multiplicative constant equal to $(R/d)^2$, where R is the radius of the star and d is the distance to the star (Cushing et al. 2008). In order to increase the S/N of the data, we first smoothed the higher resolution spectra to $R=200$. The model spectra were also smoothed to the same resolving power and linearly interpolated onto the wavelength scale of the data. For each model we compute the scale factor C_k by minimizing G_k with respect to C_k and identify the best fitting model as having the global minimum G_k value. To estimate the range of models that fits the data well, we run a Monte Carlo simulation that uses the uncertainties in the individual spectral points and the uncertainties in the absolute flux calibration of the spectra to generate 10^4 simulated noisy spectra. The fitting process is repeated on each simulated spectrum and models that are consistent with the best fitting model at the 3σ level are considered equally good representations of the data. We did not attempt to fit the spectrum of WISEP J1828+2650 because it is contaminated with light from other stars in the WFC3 field of view (see §3.2.4 and §4.1.1). After discussing the results of the fits to the spectra of the other

brown dwarfs, we return to estimate an approximate effective temperature for WISEP J1828+2650.

Table 6 lists the best fitting model parameters for each brown dwarf, as well as UGPS 0722−05. The derived effective temperatures of the WISE brown dwarfs are all cold, ranging from 350 to 500 K. Indeed all but one have estimated effective temperatures of less than 450 K making them the coldest spectroscopically confirmed brown dwarfs known. Five out of the six best fitting models also have $K_{\text{zz}}\neq0$ which indicates that vertical mixing is present in the atmospheres of these cold brown dwarfs. This is not a surprising result given that strong evidence for vertical mixing in the atmospheres of brown dwarfs has been found at longer wavelengths (Saumon et al. 2006, 2007; Leggett et al. 2007b; Burgasser et al. 2008; Leggett et al. 2009; Stephens et al. 2009; Geballe et al. 2009; Cushing et al. 2010). At such low temperatures, the effects of non-equilibrium chemistry on the J- and H-band spectra of brown dwarfs is limited to weakening the NH$_3$ absorption bands. The detection of mixing therefore underscores the fact that NH$_3$ is probably at least partially responsible for the absorption seen on the blue wing of the H-band peak of WISEPC J1405+5534 and WISEP J1738+2732.

Figure 9 shows the best fitting model spectra overplotted on the data. Since this is the first time such cold model spectra have been compared to observed spectra, the agreement between the models and the data is encouraging. In particular, the height and width of the J-band peaks are well matched by the model spectra. Previous studies of hotter brown dwarfs fail to match both the peak and width of this peak (e.g., Leggett et al. 2009; Burgasser et al. 2011). The improved fits may be a result of the fact that we are fitting a smaller wavelength range (Cushing et al. 2008; Seifahrt et al. 2009) and/or because the high J vibration-rotation lines (the so-called "hot" lines), whose cross-sections are less well known, become less important at such cold temperatures.

The models do, however, provide a poor fit to the blue wing of the H-band peak of the spectra and fail to reproduce the heights of the Y-band peaks of WISEP J0410+1502 and WISEP J1541−2250. Note that the peak of the Y-band is shaped by the $2\nu_1+2\nu_4$ band of NH$_3$ centered at about 1.03 μm and therefore Y-band spectra of cold brown dwarfs could provide the first clear detection of NH$_3$ at near-infrared wavelengths. In principle, the blue wing of the H-band model spectrum could be brought into better agreement with the data by further reducing the abundance of NH$_3$. However, as noted above, the abundance of NH$_3$ is insensitive to variations in K_{zz} because it is quenched in the convective region where the mixing time scale is set by the mixing length theory and not by the eddy diffusion coefficient. Therefore, the mismatch between the data and models is most likely a result of some other inadequacy in the model atmospheres.

Finally, although we cannot fit the models to the spectrum of WISEP J1828+2650, we can still estimate a rough effective temperature. The most salient feature of the spectrum is that the J- and H-band peaks are roughly the same height in flux density units of f_λ. Only model spectra with $T_{\text{eff}} \leq 250$ K have J-band peak fluxes that are equal to or less than the H-band peak fluxes. A second estimate of the effective tem-

perature can be derived from the observed $J-W2$ color of 9.29±0.35. We computed synthetic Mauna Kea Observatories Near-Infrared (MKO-NIR, Tokunaga et al. 2002) J and W2 magnitudes for each model in the grid and find that model spectra with $T_{\rm eff}$=275−300 K have $J-W2$ colors that fall within ±2σ of the observed color. Taken together, these estimates suggest that an appropriate upper limit to the effective temperature of WISEP J1828+2650 is ∼300 K which makes WISEP J1828+2650 the coolest spectroscopically confirmed brown dwarf known.

4.2.2. *Structural Properties*

With estimates of the effective temperatures and surface gravities of the new brown dwarfs in hand, we can also estimate their radii (R) and masses (M) using evolutionary models. We used the cloudless structure models of Saumon & Marley (2008) because they used atmospheric models that are nearly identical to the ones we used in our analysis for boundary conditions. As a result, the derived $T_{\rm eff}$, $\log g$, R, and M estimates are all self-consistent. The radii and masses of the brown dwarfs are given in Table 6.

4.3. *Spectroscopic Distance Estimates*

The value of the multiplicative constant C_k=$(R/d)^2$ derived as a by product of the atmospheric model fitting procedure can be used to estimate a so-called "spectroscopic distance" ($d_{\rm spec}$) to brown dwarfs if their radii can be determined (e.g., Bowler et al. 2009). In the absence of direct measurements of brown dwarf radii, we can use the radii computed using evolutionary models and ($T_{\rm eff}$, $\log g$) values. The spectroscopic distances of the new WISE brown dwarfs and UGPS 0722−05 are given in Table 7. Also listed in Table 7 are the photometric distance estimates of the WISE brown dwarfs from Kirkpatrick et al. (2011) and parallactic distances to UGPS 0722−05 (Lucas et al. 2010) and WISEP J1541−2250 (Kirkpatrick et al. 2011). The former distance estimates are computed using a spectral type-W2 relation derived from known brown dwarfs with spectral types ranging from L0 to T9 and with $\pi/\sigma_\pi >$ 3. The photometric distances of the new WISE brown dwarfs are based on an *extrapolation* of this relation and therefore should be treated with caution.

The agreement between the three distance estimates range from good to poor. For example, the spectroscopic and parallactic distances of WISEP J1541−2250 are in good agreement but the photometric distance is discrepant by a factor of two to four. Perhaps most discouraging is the mismatch between the spectroscopic and parallactic distances of UGPS 0722−05. Liu et al. (2011) recently showed that the agreement between the spectroscopic distances (derived using only near-infrared spectra) and the parallactic distances of ten late-type T dwarfs range from 10% to a factor of two, with no apparent trend with spectral type or distance. This suggests that spectroscopic distances should only be used to confirm that the physical properties of brown dwarfs ($T_{\rm eff}$, R, M) derived from atmospheric and evolutionary models are consistent with the known distance to the brown dwarf.

A corollary to this statement is that if the spectroscopic and parallactic distances are discrepant then some com-

bination of the $T_{\rm eff}$, $\log g$ and R values are in error. In order to estimate the significance of the bias in the spectroscopic distance estimate introduced by systematic errors in the inferred atmospheric properties, we have run a 1−2.5 μm model with $T_{\rm eff}$=600 K, $\log g$=4.5 cm s^{-2} through the fitting procedure described in §4.2.1. The model spectrum was first multiplied by an appropriate value of $(R/d)^2$ corresponding to 10 pc. Figure 10 shows the ratio of $d_{\rm spec}$/ 10 pc derived for models with effective temperatures from 500 to 700 K and surface gravities from 3.75 to 5.0. The maximum change in $d_{\rm spec}$ for these models is approximately a factor of two for a change of +100 K/−0.75 dex and −100 K/+0.5 dex in $T_{\rm eff}$/$\log g$. The spectroscopic distance is also most sensitive to changes in $T_{\rm eff}$ as noted by Liu et al. (2011).

The apparent mismatch between the spectroscopic and parallactic distance estimates is perhaps not so surprising as Cushing et al. (2008) have shown that variations of order 100 to 200 K are common when estimating the effective temperatures of L and early- to mid-type T dwarfs using spectra that cover only a fraction of the spectral energy distribution. These variations are most likely exacerbated by the fact that only ∼35% (in flux density units of f$_\lambda$) of the bolometric flux of a $T_{\rm eff}$=600 K brown dwarf is emitted at near-infrared wavelengths. In summary, given the uncertainties in the model atmospheres and the difficulty in estimating the effective temperatures and surface gravities of brown dwarfs, it is not surprising that spectroscopic distance estimates do not always agree with the parallactic distances.

5. DISCUSSION

The new WISE brown dwarfs presented herein are the coldest ($T_{\rm eff}$=300−500 K) spectroscopically confirmed brown dwarfs currently known. However as noted in §1, WD 0806−661B and CFBDSIR J1458+1013B have estimated effective temperatures of ∼300−400 K based on photometry alone (Luhman et al. 2011; Liu et al. 2011; Rodriguez et al. 2011). How do the properties of these two brown dwarfs compare with the new WISE brown dwarfs?

The upper panel of Figure 11 shows the absolute J-band magnitude (M_J) as a function of spectral type for a sample of field T dwarfs (Leggett et al. 2010), WISEP J1541−2250 (the only WISE brown dwarf with a measured parallax), WD 0806−661B (Luhman et al. submitted) and CFBDSIR J1458+1013B (Liu et al. 2011). The value of M_J increases precipitously beyond a spectral type of T8 and reaches ∼23.9 for WISEP J1541−2250 (Y0). The absolute magnitude of CFBDSIR J1458+1013B falls between the two T9 dwarfs and WISEP J1541−2250 suggesting that it has a spectral type of T9−Y0. However the absolute magnitudes of more late-type T dwarfs and Y dwarfs must be measured before any strong conclusions can be drawn based on absolute magnitudes alone. The absolute magnitude of WD 0806−661B is still only a limit ($M_J > 22.5$) which leaves open the possibility that WD 0806−661B is even fainter, and thus presumably cooler than, WISEP J1541−2250. Either way, it is clear that based on the trend of M_J with spectral type that observing even colder objects at near-infrared wavelengths is going to become increasingly difficult unless they are very close the Sun.

The lower panel of Figure 11 shows the $J-H$ col-

ors as a function of spectral type for a sample of field T dwarfs (Leggett et al. 2010), the new WISE brown dwarfs, and CFBDSIR J1458+1013B (WD 0806−661B has yet to be detected in either the J or H band). Some of the colors of the WISE brown dwarfs have large uncertainties so we also computed synthetic MKO-NIR $J - H$ colors as described in Rayner et al. (2009); they are shown as triangles in Figure 11. Since the WFC3/HST spectra do not span the entire H band, we used the spectrum of UGPS 0722−05 to extend the spectra of WISEP J1738+2732 and WISEPC J1405+5534 to the limit of the H band filter. The synthetic and observed photometry of WISEPC J1405+5534 are clearly discrepant and it is unclear what the underlying cause is. The scatter in the $J - H$ colors of the dwarfs at the T/Y transition makes it difficult to assign a spectral type to CFBDSIR J1458+1013B but it is broadly consistent with T6−Y0. The overall trend with spectral type suggests suggests that the $J - H$ colors may be turning towards to the red at the T/Y transition. This turn is broadly consistent with theoretical models which predict that the $J - K$ color also turns towards the red at T_{eff}=390−450 K (Burrows et al. 2003). However given the small number of objects and the large uncertainties in colors, a definitive conclusion can not yet be reached.

Finally, given the rapid increase in the absolute J-band magnitude at the T/Y transition, it is reasonable to ask whether the near-infrared is the appropriate wavelength range with which to define the Y spectral class. Indeed historically as cooler and cooler stars were discovered, the wavelength range used for spectral classification moved from the blue violet at 3900−4900 Å (Morgan et al. 1943), through the red optical at 7000−10000 Å (Boeshaar 1976; Kirkpatrick et al. 1991, 1999), and finally into the near infrared at 1−2.5 μm (Burgasser et al. 2006). Since Y dwarfs emit the majority of their flux in the mid-infrared, it seems only natural to devise the spectral classification system at these wavelengths. The smooth spectral morphological changes seen in the 5.5−14.5 μm $Spitzer$ spectra of L and T dwarfs (Cushing et al. 2006) suggest that a mid-infrared classification scheme for the Y dwarfs is plausible. Unfortunately, observing at wavelengths longer about 2.5 μm from the ground is exceedingly difficult due to the high thermal background. Observations conducted from space do not suffer from this limitation but there are currently no space-based facilities (including $Spitzer$) capable of obtaining mid-infrared spectra of cold brown dwarfs. The $James Webb Space Telescope$ will provide a platform with which to observe cold brown dwarfs (Burrows et al. 2003; Marley & Leggett 2009) but its launch is, at best, still years away.

We are therefore left in the unfortunate position of either waiting for a (space- or ground-based) facility capable of sensitive mid-infrared observations or constructing a classification scheme in the near infrared. Given the large number of cold brown dwarfs now known, we believe it is important to devise a system with which to classify them based on the data currently available. The creation of a near-infrared scheme in no way invalidates any future mid-infrared system that may be devised. Indeed the classification of brown dwarfs at two different wavelengths is not unprecedented as both the L and the

T dwarfs have classification systems based in the red optical (Kirkpatrick et al. 1999; Burgasser et al. 2003) and the near infrared (Geballe et al. 2002; Kirkpatrick et al. 2010; Burgasser et al. 2006). Ultimately, the utility of any classification system will be measured by whether or not it is adopted by the brown dwarf community.

6. SUMMARY

As part of an ongoing search for the coldest brown dwarfs in the solar neighborhood using the Wide-field Infrared Survey Explorer, we have discovered seven ultracool brown dwarfs whose near-infrared spectra indicate that they are the latest-type brown dwarfs currently known. Based on the spectral morphological differences between these brown dwarfs and the late-type T dwarfs, we have identified six of them as the first members of the Y spectral class. A comparison to the model spectra of Marley & Saumon indicate that they have effective temperatures ranging from 300 to 500 K and thus are the coldest spectroscopically confirmed brown dwarfs currently known.

REFERENCES

Allen, P. R., Koerner, D. W., Reid, I. N., & Trilling, D. E. 2005, ApJ, 625, 385

Bertin, E., & Arnouts, S. 1996, A&AS, 117, 393

Beuzit, J. L., et al. 2006, in Tenth Anniversary of 51 Peg-b: Status of and prospects for hot Jupiter studies, ed. L. Arnold, F. Bouchy, & C. Moutou, 353–355

Boeshaar, P. C. 1976, PhD thesis, Ohio State University, Columbus.

Bowler, B. P., Liu, M. C., & Cushing, M. C. 2009, ApJ, 706, 1114

Burgasser, A. J. 2004, ApJS, 155, 191

Burgasser, A. J., et al. 2011, ApJ, 735, 116

Burgasser, A. J., Geballe, T. R., Leggett, S. K., Kirkpatrick, J. D., & Golimowski, D. A. 2006, ApJ, 637, 1067

Burgasser, A. J., Kirkpatrick, J. D., Liebert, J., & Burrows, A. 2003, ApJ, 594, 510

Burgasser, A. J., et al. 2010, ApJ, 725, 1405

Burgasser, A. J., Tinney, C. G., Cushing, M. C., Saumon, D., Marley, M. S., Bennett, C. S., & Kirkpatrick, J. D. 2008, ApJ, 689, L53

Burningham, B., et al. 2011a, MNRAS, 414, 3590

—. 2011b, MNRAS, 414, L90

—. 2008, MNRAS, 391, 320

—. 2009, MNRAS, 395, 1237

—. 2010, MNRAS, 406, 1885

Burrows, A., & Sharp, C. M. 1999, ApJ, 512, 843

Burrows, A., Sudarsky, D., & Lunine, J. I. 2003, ApJ, 596, 587

Chauvin, G., Lagrange, A., Dumas, C., Zuckerman, B., Mouillet, D., Song, I., Beuzit, J., & Lowrance, P. 2004, A&A, 425, L29

Cushing, M. C., et al. 2008, ApJ, 678, 1372

Cushing, M. C., Rayner, J. T., & Vacca, W. D. 2005, ApJ, 623, 1115

Cushing, M. C., et al. 2006, ApJ, 648, 614

Cushing, M. C., Saumon, D., & Marley, M. S. 2010, AJ, 140, 1428

Delorme, P., et al. 2008a, A&A, 482, 961

—. 2008b, A&A, 484, 469

Epchtein, N., et al. 1997, The Messenger, 87, 27

Fazio, G. G., et al. 2004, ApJS, 154, 10

Freedman, R. S., Marley, M. S., & Lodders, K. 2008, ApJS, 174, 504

Geballe, T. R., et al. 2002, ApJ, 564, 466

Geballe, T. R., Saumon, D., Golimowski, D. A., Leggett, S. K., Marley, M. S., & Noll, K. S. 2009, ApJ, 695, 844

Hanel, R., Conrath, B., Herath, L., Kunde, V., & Pirraglia, J. 1981, J. Geophys. Res., 86, 8705

Hayashi, C., & Nakano, T. 1963, Progress of Theoretical Physics, 30, 460

Hinkley, S., et al. 2011, PASP, 123, 74

Hubeny, I., & Burrows, A. 2007, ApJ, 669, 1248

Kimble, R. A., MacKenty, J. W., O'Connell, R. W., & Townsend, J. A. 2008, in Presented at the Society of Photo-Optical Instrumentation Engineers (SPIE) Conference, Vol. 7010, Society of Photo-Optical Instrumentation Engineers (SPIE) Conference Series

Kirkpatrick, J. D. 2000, in Astronomical Society of the Pacific Conference Series, Vol. 212, From Giant Planets to Cool Stars, ed. C. A. Griffith & M. S. Marley, 20

Kirkpatrick, J. D. 2008, in Astronomical Society of the Pacific Conference Series, Vol. 384, 14th Cambridge Workshop on Cool Stars, Stellar Systems, and the Sun, ed. G. van Belle, 85

Kirkpatrick, J. D., et al. 2011, ApJS

Kirkpatrick, J. D., Henry, T. J., & McCarthy, Jr., D. W. 1991, ApJS, 77, 417

Kirkpatrick, J. D., et al. 2010, ApJS, 190, 100

—. 1999, ApJ, 519, 802

Koekemoer, A. M., Fruchter, A. S., Hook, R. N., & Hack, W. 2002, in The 2002 HST Calibration Workshop : Hubble after the Installation of the ACS and the NICMOS Cooling System, ed. S. Arribas, A. Koekemoer, & B. Whitmore, 337

Kumar, S. S. 1963, ApJ, 137, 1121

Kümmel, M., Walsh, J. R., Pirzkal, N., Kuntschner, H., & Pasquali, A. 2009, PASP, 121, 59

Lawrence, A., et al. 2007, MNRAS, 379, 1599

Leggett, S. K., et al. 2010, ApJ, 710, 1627

—. 2009, ApJ, 695, 1517

Leggett, S. K., Marley, M. S., Freedman, R., Saumon, D., Liu, M. C., Geballe, T. R., Golimowski, D. A., & Stephens, D. C. 2007a, ApJ, 667, 537

Leggett, S. K., Saumon, D., Marley, M. S., Geballe, T. R., Golimowski, D. A., Stephens, D., & Fan, X. 2007b, ApJ, 655, 1079

Liu, M. C., et al. 2011, ArXiv e-prints

Lodders, K. 1999, ApJ, 519, 793

Lodders, K., & Fegley, B. 2002, Icarus, 155, 393

Lucas, P. W., et al. 2010, MNRAS, 408, L56

Luhman, K. L., Adame, L., D'Alessio, P., Calvet, N., Hartmann, L., Megeath, S. T., & Fazio, G. G. 2005, ApJ, 635, L93

Luhman, K. L., Burgasser, A. J., & Bochanski, J. J. 2011, ApJ, 730, L9

Macintosh, B., et al. 2006, in Presented at the Society of Photo-Optical Instrumentation Engineers (SPIE) Conference, Vol. 6272, Society of Photo-Optical Instrumentation Engineers (SPIE) Conference Series

Mainzer, A., et al. 2011, ApJ, 726, 30

Marley, M. S., & Leggett, S. K. 2009, The Future of Ultracool Dwarf Science with JWST, ed. Thronson, H. A., Stiavelli, M., & Tielens, A., 101

Marley, M. S., Seager, S., Saumon, D., Lodders, K., Ackerman, A. S., Freedman, R. S., & Fan, X. 2002, ApJ, 568, 335

Martini, P., Persson, S. E., Murphy, D. C., Birk, C., Shectman, S. A., Gunnels, S. M., & Koch, E. 2004, in Society of Photo-Optical Instrumentation Engineers (SPIE) Conference Series, Vol. 5492, Society of Photo-Optical Instrumentation Engineers (SPIE) Conference Series, ed. A. F. M. Moorwood & M. Iye, 1653–1660

McLean, I. S., et al. 1998, in Society of Photo-Optical Instrumentation Engineers (SPIE) Conference Series, Vol. 3354, Society of Photo-Optical Instrumentation Engineers (SPIE) Conference Series, ed. A. M. Fowler, 566–578

McLean, I. S., Graham, J. R., Becklin, E. E., Figer, D. F., Larkin, J. E., Levenson, N. A., & Teplitz, H. I. 2000, in Society of Photo-Optical Instrumentation Engineers (SPIE) Conference Series, Vol. 4008, Society of Photo-Optical Instrumentation Engineers (SPIE) Conference Series, ed. M. Iye & A. F. Moorwood, 1048–1055

McLean, I. S., McGovern, M. R., Burgasser, A. J., Kirkpatrick, J. D., Prato, L., & Kim, S. S. 2003, ApJ, 596, 561

Morgan, W. W., Keenan, P. C., & Kellman, E. 1943, An atlas of stellar spectra, with an outline of spectral classification, ed. Morgan, W. W., Keenan, P. C., & Kellman, E.

Rayner, J. T., Cushing, M. C., & Vacca, W. D. 2009, ApJS, 185, 289

Rayner, J. T., Toomey, D. W., Onaka, P. M., Denault, A. J., Stahlberger, W. E., Vacca, W. D., Cushing, M. C., & Wang, S. 2003, PASP, 115, 362

Rodriguez, D. R., Zuckerman, B., Melis, C., & Song, I. 2011, ApJ, 732, L29

Roellig, T. L., et al. 2004, ApJS, 154, 418

Saumon, D., Geballe, T. R., Leggett, S. K., Marley, M. S., Freedman, R. S., Lodders, K., Fegley, Jr., B., & Sengupta, S. K. 2000, ApJ, 541, 374

Saumon, D., & Marley, M. S. 2008, ApJ, 689, 1327

Saumon, D., Marley, M. S., Cushing, M. C., Leggett, S. K., Roellig, T. L., Lodders, K., & Freedman, R. S. 2006, ApJ, 647, 552

Saumon, D., et al. 2007, ApJ, 656, 1136

Saumon, D., Marley, M. S., Lodders, K., & Freedman, R. S. 2003, in IAU Symposium, Vol. 211, Brown Dwarfs, ed. E. Martín, 345

Seifahrt, A., et al. 2009, in American Institute of Physics Conference Series, Vol. 1094, American Institute of Physics Conference Series, ed. E. Stempels, 283–290

Simcoe, R. A., et al. 2008, in Presented at the Society of Photo-Optical Instrumentation Engineers (SPIE) Conference, Vol. 7014, Society of Photo-Optical Instrumentation Engineers (SPIE) Conference Series

Simcoe, R. A., et al. 2010, in Society of Photo-Optical Instrumentation Engineers (SPIE) Conference Series, Vol. 7735, Society of Photo-Optical Instrumentation Engineers (SPIE) Conference Series

Skrutskie, M. F., et al. 2006, AJ, 131, 1163

Skrutskie, M. F., et al. 2010, in Society of Photo-Optical
    Instrumentation Engineers (SPIE) Conference Series, Vol. 7735,
    Society of Photo-Optical Instrumentation Engineers (SPIE)
    Conference Series
Stephens, D. C., et al. 2009, ApJ, 702, 154
Tokunaga, A. T., Simons, D. A., & Vacca, W. D. 2002, PASP,
    114, 180
van Dam, M. A., et al. 2006, PASP, 118, 310
Warren, S. G., & Brandt, R. E. 2008, Journal of Geophysical
    Research (Atmospheres), 113, D14220
Warren, S. J., et al. 2007, MNRAS, 381, 1400
Weights, D. J., Lucas, P. W., Roche, P. F., Pinfield, D. J., &
    Riddick, F. 2009, MNRAS, 392, 817, erratum
Werner, M. W., et al. 2004, ApJS, 154, 1

Whitworth, A., Bate, M. R., Nordlund, Å., Reipurth, B., &
    Zinnecker, H. 2007, Protostars and Planets V, 459
Whitworth, A. P., & Stamatellos, D. 2006, A&A, 458, 817
Wilson, J. C., et al. 2003, in Society of Photo-Optical
    Instrumentation Engineers (SPIE) Conference Series, Vol. 4841,
    Society of Photo-Optical Instrumentation Engineers (SPIE)
    Conference Series, ed. M. Iye & A. F. M. Moorwood, 451–458
Wizinowich, P. L., et al. 2006, PASP, 118, 297
Wright, E. L., et al. 2010, AJ, 140, 1868
York, D. G., et al. 2000, AJ, 120, 1579
Yurchenko, S. N., Barber, R. J., & Tennyson, J. 2010, ArXiv
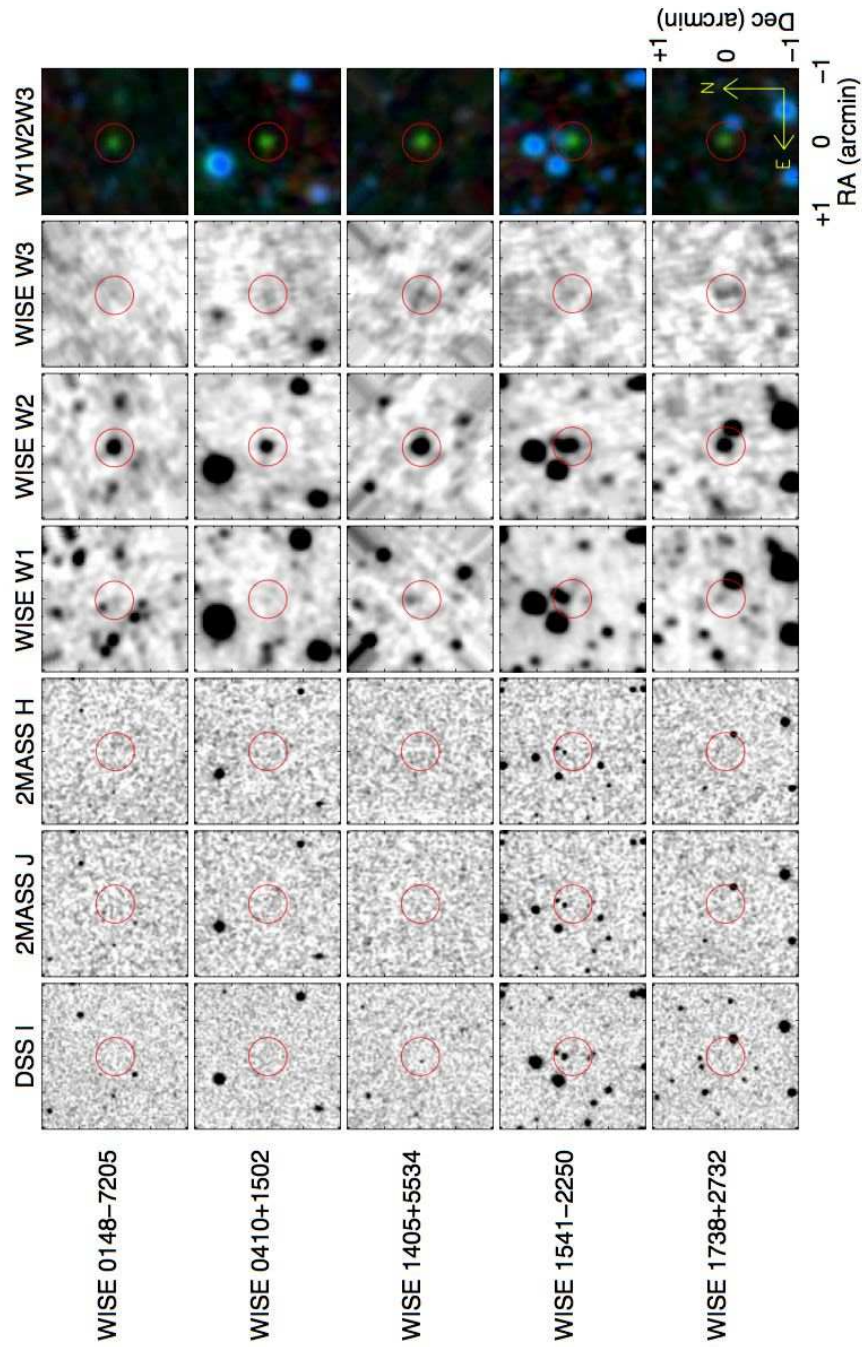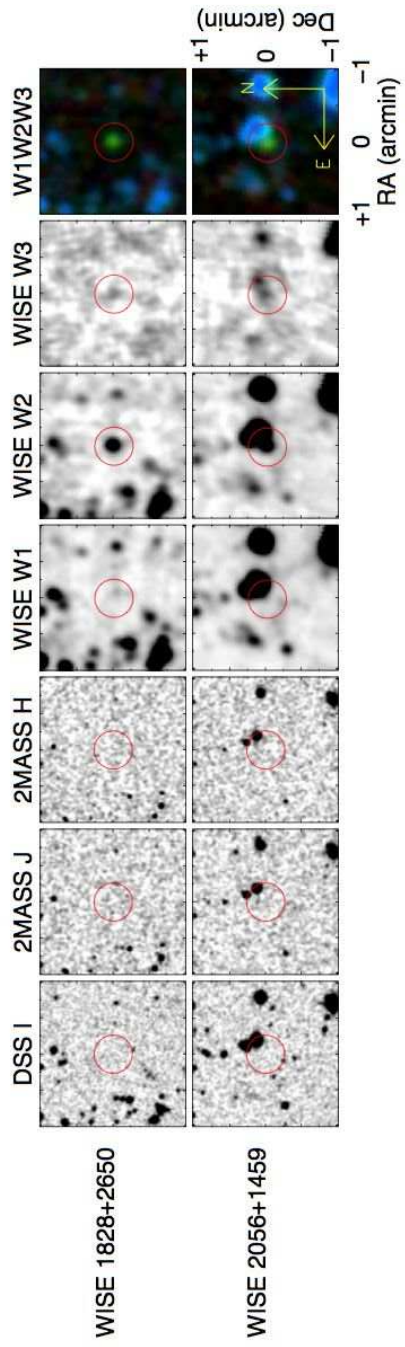   e-prints
—. 2011, MNRAS, 413, 1828

FIG. 1.— 2 × 2 arcmin DSS I, 2MASS J and H, WISE W1, W2, and W3, and a W1W2W3 false color composite of the five new WISE brown dwarfs. In the color composite images on the far right, the W1, W2, and W3 are bands are color coded blue, green, and red, respectively.
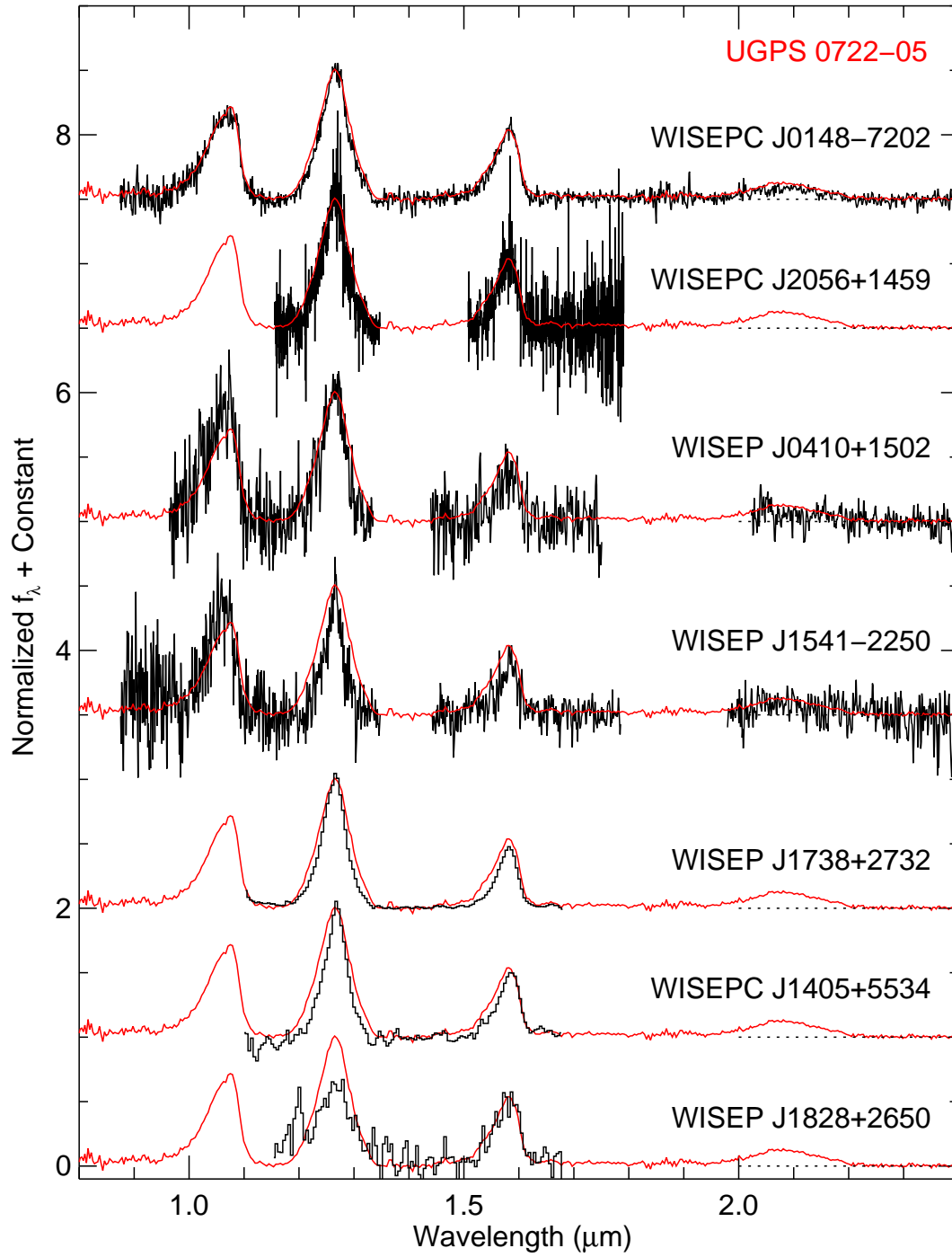
FIG. 2.— Near-infrared spectra of the new WISE brown dwarfs (black) as compared to the spectrum of UGPS 0722−05 (red). The data have been normalized to unity at the peak of the *J* band (except for WISEP J1828+2650 which is normalized to unity at the peak of the *H*-band) and offset by constants (dotted lines).
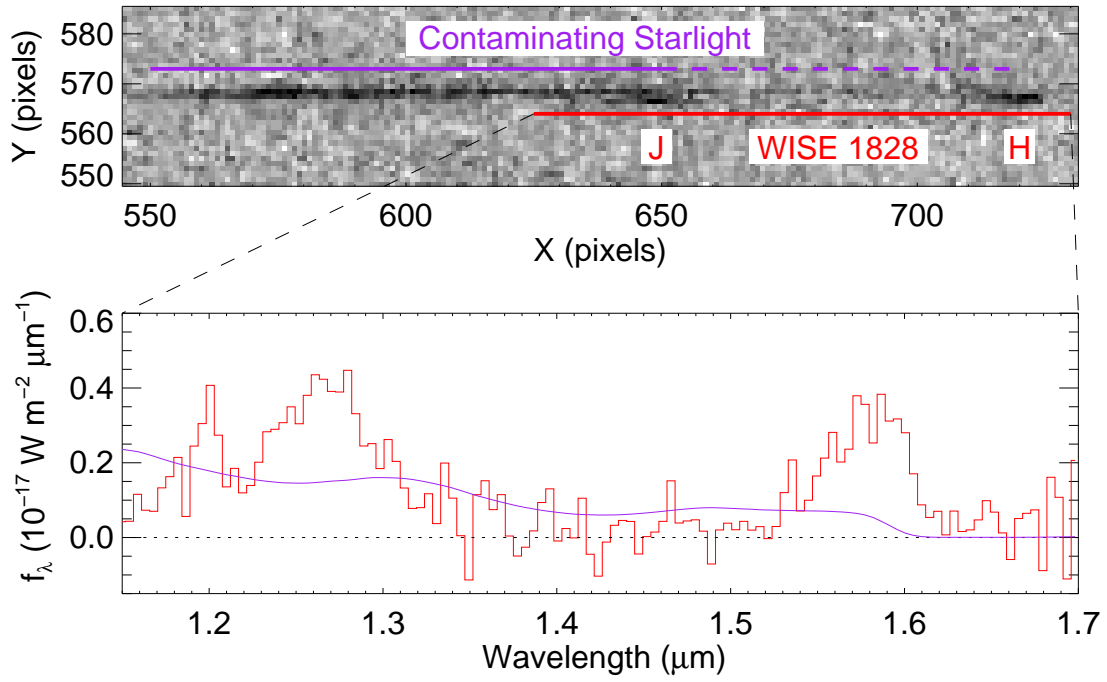
FIG. 3.— Top: Subimage of the drizzled WFC3/HST grism image centered on the position of WISEP J1828+2650. The location of the spectrum of WISEP J1828+2650 is indicated in red along with the positions of the J- and H-band peaks. The location of the contaminating starlight is shown in purple and consists of second and third order light from two other stars in the WFC3 field of view. Bottom: The spectrum of WISEP J1828+2650 (red) and the contamination spectrum (purple). The stellar contamination becomes progressively worse at shorter wavelengths.

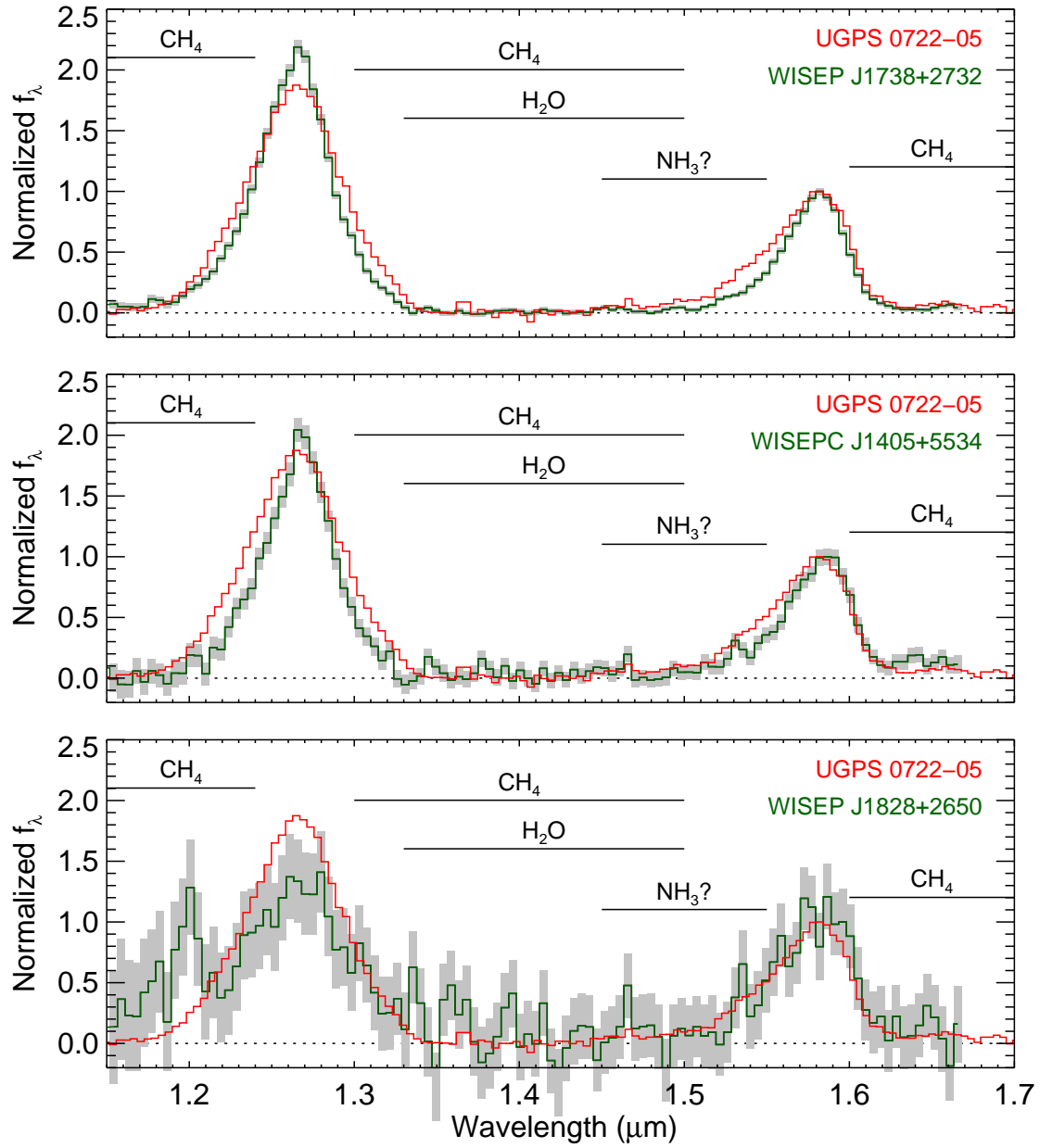FIG. 4.— 1.15−1.70 µm spectra of WISEP J1738+2732, WISEPC J1405+5534, and WISEP J1828+2650 along with the spectrum UGPS 0722−05. The uncertainties in the spectra are shown as gray bars. The spectra were all normalized to unity at the peak of the H-band (1.58 µm). Prominent molecular absorption bands are indicated.
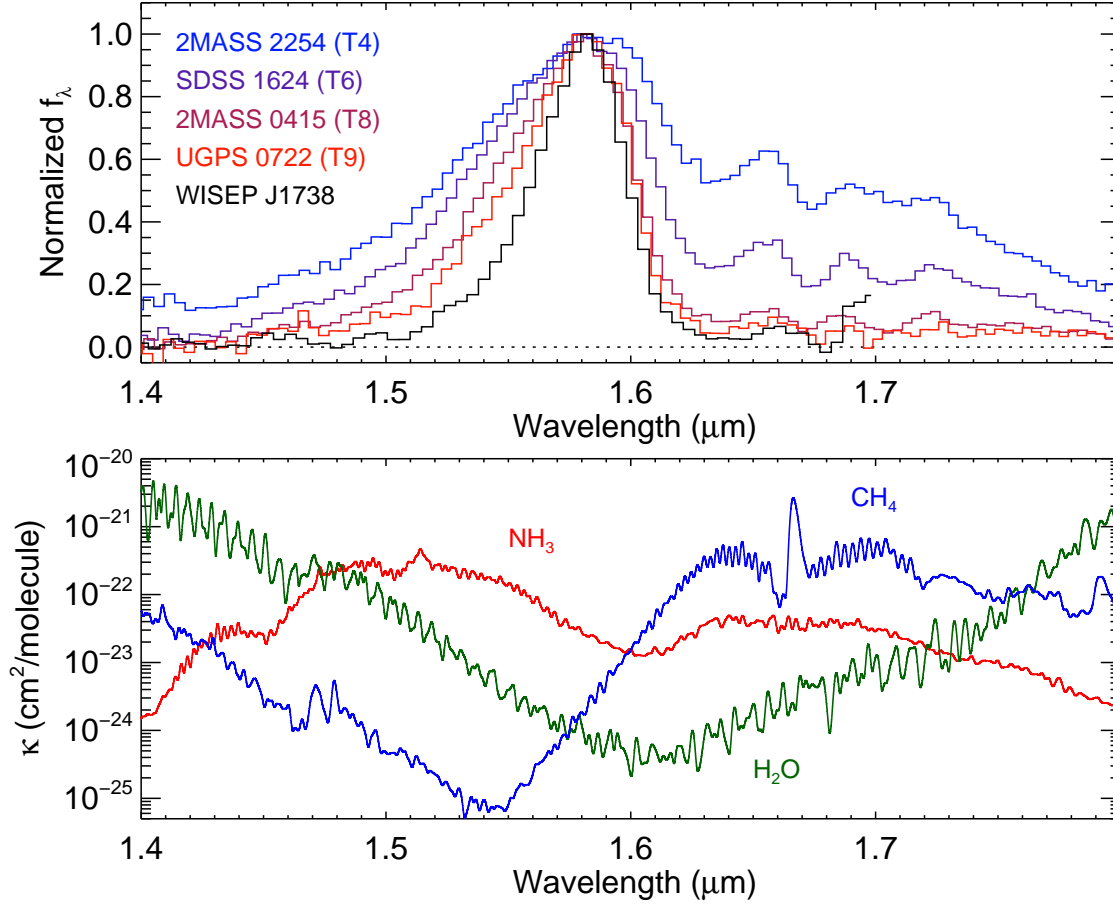
Fig. 5.— Top: H-band spectrum of 2MASS J22541892+3123498, SDSS J162414.37+002915.6 and 2MASS J04151954−0935066, the T4, T6, and T8 spectral standards (Burgasser et al. 2006), along with the spectrum of UGPS 0722−05, and WISEP J1738+2732. The spectra have been normalized to unity at their peak flux values. Bottom: Opacity data computed in chemical equilibrium for NH$_3$ (Yurchenko et al. 2010), H$_2$O (Freedman et al. 2008), and CH$_4$ (Freedman et al. 2008) at T=600 K and P=1 bar. Note that the change in the spectral morphology of the blue wing of the H-band peak is similar between T6/T8 and T8/T9 suggesting a common absorber or set of absorbers. In contrast, the spectrum of WISEP J1738+2732 exhibits excess absorption that matches the position of the NH$_3$ absorption shown in the lower panel.
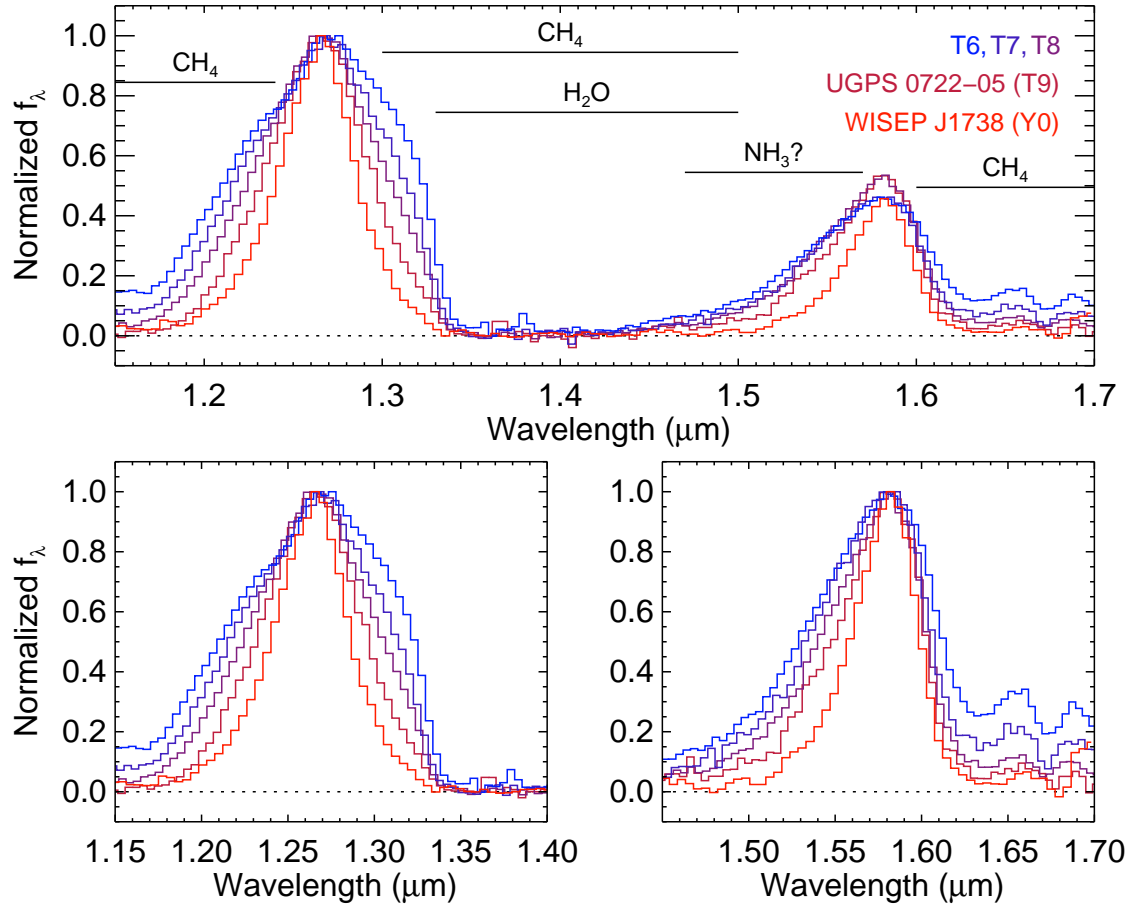
F𝘪ɢ. 6.— IRTF/SpeX spectra of the Burgasser et al. (2006) spectral standards, SDSS J162414.37+002915.6 (T6), 2MASS J07271824+1710012 (T7), and 2MASS J04151954−0935066 (T8), our IRTF/SpeX spectrum of UGPS 0722−05 and the WFC3/*HST* spectrum of WISEP J1738+2732. The spectra have been normalized to unity at their peak flux level in each panel. Prominent molecular absorption bands are indicated in the top panel.
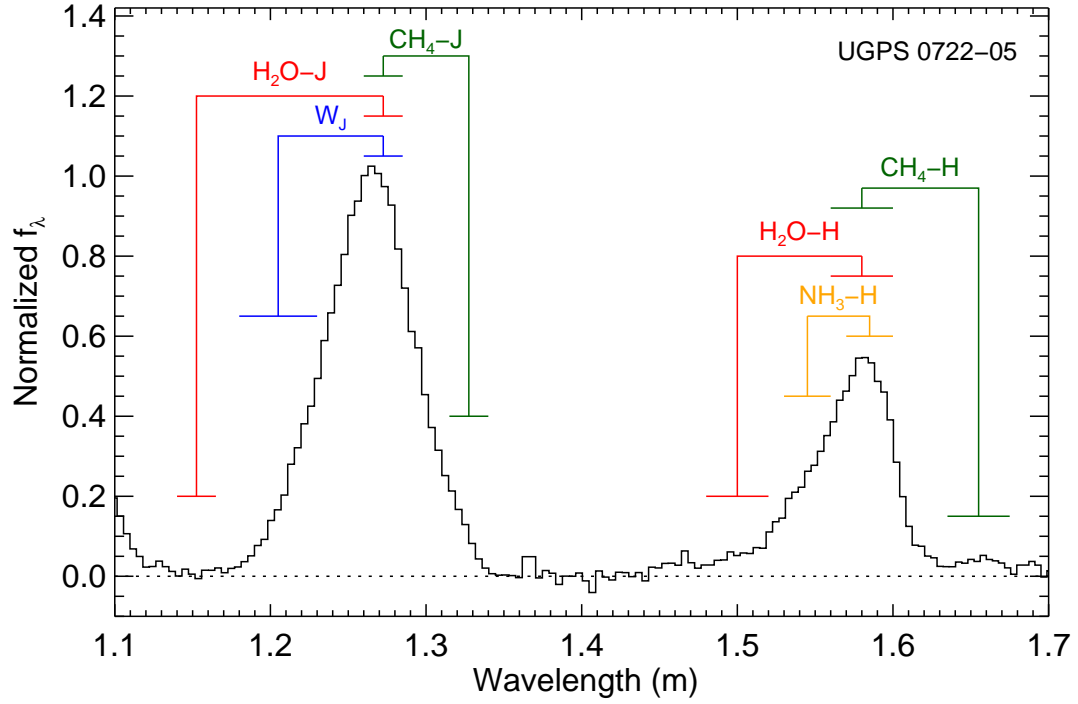
FIG. 7.— Illustration of the H_2O-J, W_J, CH_4-J, CH_4-J, NH_3-H, and CH_4-H indices overplotted on the spectrum UGPS 0722-05.
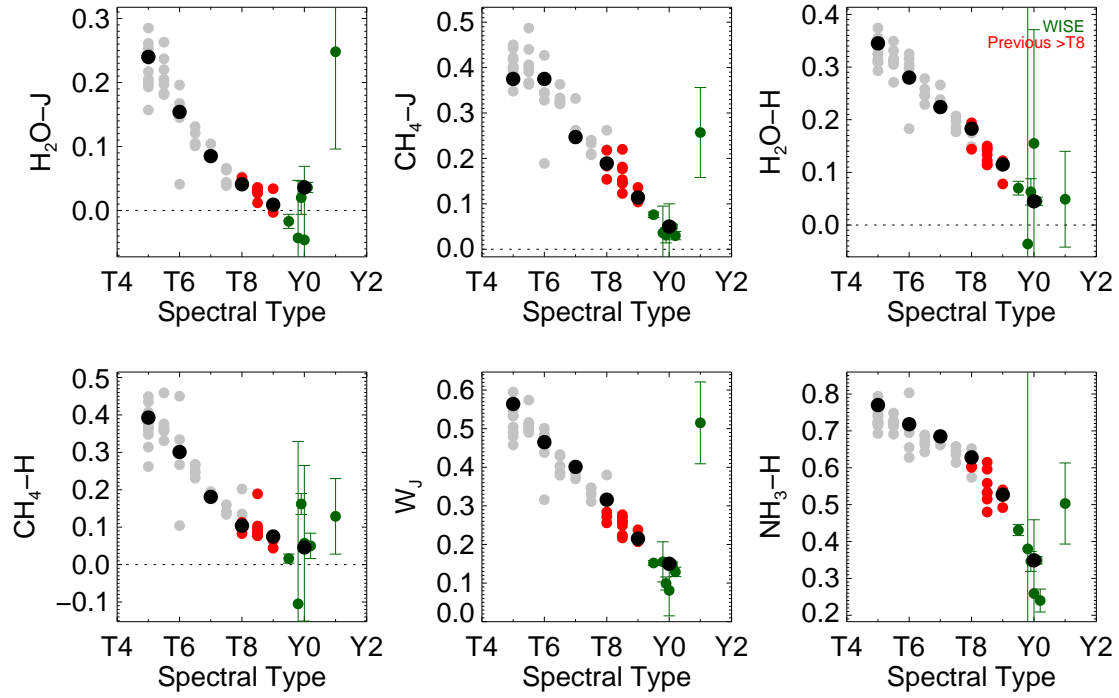
FIG. 8.— Values of the H₂O−J, CH₄−J, H₂O−H, CH₄−H (Burgasser et al. 2006), W_J (Warren et al. 2007), and NH₃−H (Delorme et al. 2008a) spectral indices as a function of spectral type. The black points are for the T6−Y0 spectral standards. The grey points were computed using spectra of late-type (T5−T8) T dwarfs from the SpeX Prism Spectral Library. The red points are the twelve T dwarfs with previously published spectral types later than T8 and the green points are the remaining six WISE brown dwarfs. For plotting purposes only, we have assigned WISEP J1828+2650 a spectral type of Y1.
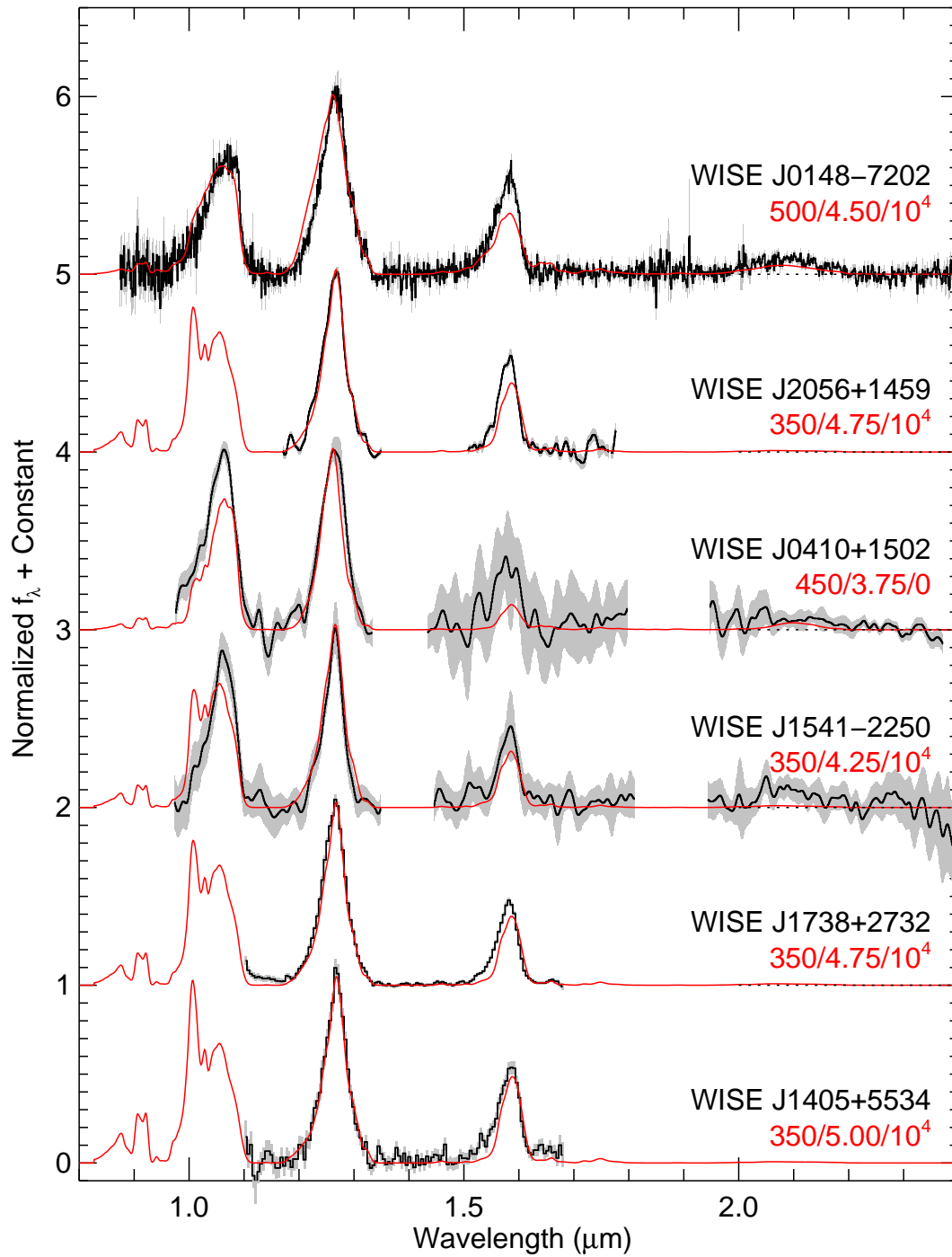
FIG. 9.— Best fitting models (red) overplotted on the near-infrared spectra of six of the seven new WISE brown dwarfs (black). The spectra were normalized to unity at the peak flux in the J-band and offset by constants (dotted lines). The uncertainties in the spectra are given by grey bars. The best fitting model parameters are given in the form $T_{\rm eff}({\rm K})/\log g \; ({\rm cm \; s^{-2}})/K_{\rm zz} \; ({\rm cm^2 \; s^{-1}})$.
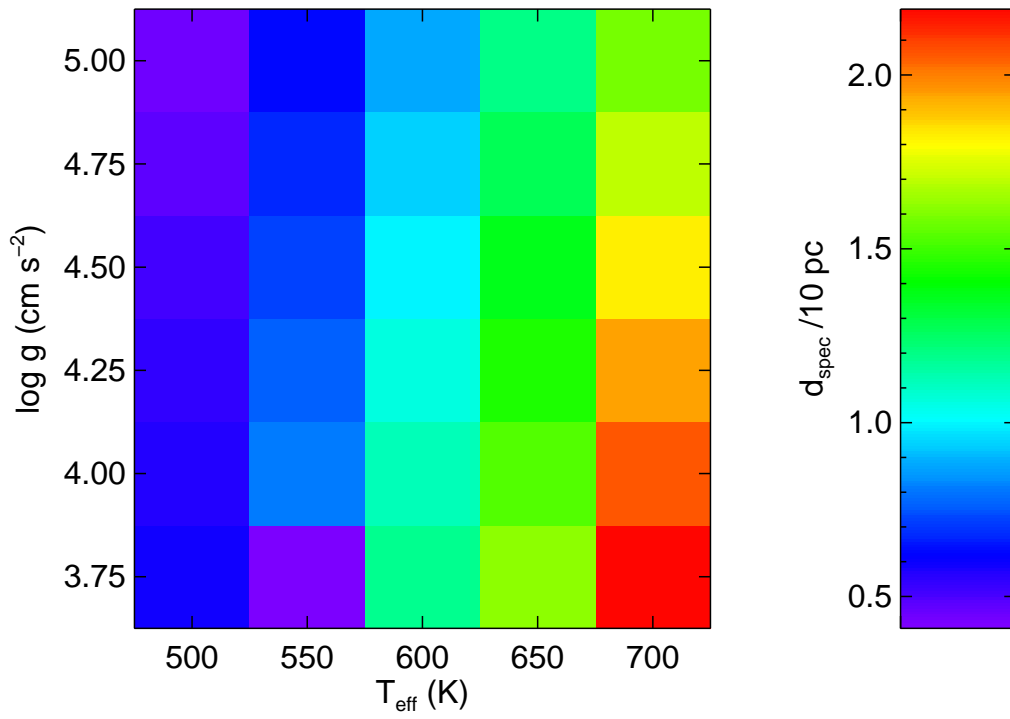
FIG. 10.— Impact of systematic errors in the derived values of $(T_{\rm eff}, \log g)$ on the spectroscopic distance, $d_{\rm spec}$, for a hypothetical dwarf with $T_{\rm eff}=600$ K and $\log g= 4.5$ cm s^{-2}.
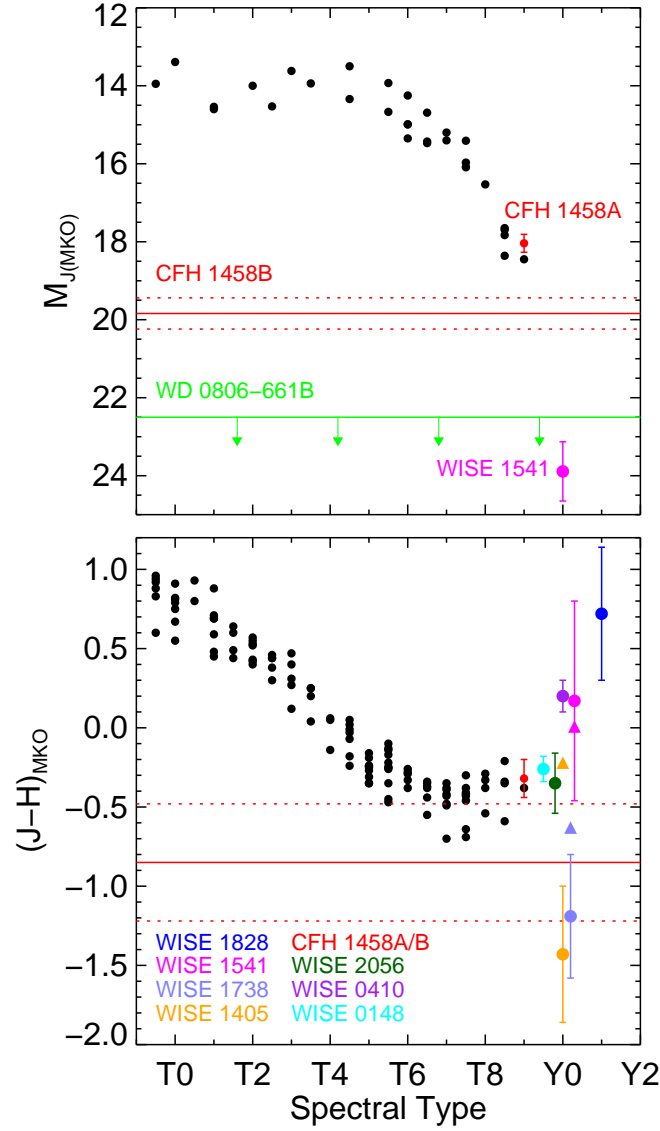
FIG. 11.— Comparison of the absolute J-band magnitudes and $J - H$ colors of the WISE brown dwarfs, WD 0806−661B, and CFBDSIR J1458+1013B. The field population (black circles) is from the compilation of Leggett et al. (2010) and the spectral types of the late-type T dwarfs have been changed to match the subtypes given in Table 5. Synthetic colors computed by integrating the J and H bandpasses over spectra are plotted as triangles. For plotting purposes only, we have assigned a spectral type of Y1 for WISEP J1828+2650.

TABLE 1
WISE Photometry

Object	W1 (mag)	W2 (mag)	W3 (mag)	W4 (mag)	W1−W2 (mag)
WISEPC J014807.25−720258.8	18.812±0.529[a]	14.584±0.052	>12.579	>9.521	4.228±0.532
WISEP J041022.71+150248.5	>18.101	14.190±0.059	12.472±0.482[a]	>8.923	>3.911±0.059
WISEPC J140518.40+553421.5	>17.989	14.085±0.041	12.312±0.252	>9.115	>3.904±0.041
WISEP J154151.65−225025.2	>17.018	13.982±0.112	12.134±0.443[a]	>9.064	>3.036±0.112
WISEP J173835.52+273258.9	18.155±0.362	14.535±0.057	12.536±0.350	>9.182	3.620±0.366
WISEP J182831.08+265037.8	>18.452	14.276±0.050	12.320±0.291	9.147±0.438[a]	>4.176±0.050
WISEPC J205628.90+145953.3	>17.742	13.852±0.043	11.791±0.222	>8.646	>3.890±0.043

Note. — Objects designated as WISEP are from the Preliminary Release Source Catalog while objects designated as WISEPC are from the first-pass processing operations coadd Source Working Database. Magnitudes are in the Vega system and are based on profile fits (w1mpro, w2mpro, w3mpro, w4mpro). Upper limits are at the 95% confidence level (see http://wise2.ipac.caltech.edu/docs/release/prelim/expsup/sec4_3c.html#ul2).

[a] S/N≤3

TABLE 2
Near-Infrared Photometry

Object	Filter	Instrument	Magnitude (mag)	Exposure Time (sec)	Coadds	Number of Images	Total Exp. (sec)	Date (UT)
WISEPC J0148−7202	J	PANIC	18.96±0.07	30	1	18	540	2010 Aug 01
	H	PANIC	19.22±0.04	15	1	108	1620	2010 Aug 01
WISEP J0410+1502	J	WIRC	19.25±0.05	60	1	15	900	2010 Aug 29
	H	WIRC	19.05±0.09	30	4	15	1800	2010 Jul 26
WISEPC J1405+5534	J	WIRC	20.20±0.13	30	2	15	1800	2010 Jul 26
	H	WIRC	21.45±0.41	⋯	⋯	⋯	5400	multiple
WISEP J1541−2250	J	NEWFIRM	21.16±0.36	30	2	10	600	2011 Apr 17
	H	NEWFIRM	20.99±0.52	5	12	10	600	2011 Apr 17
WISEP J1738+2732	J	WIRC	19.47±0.08	60	1	15	900	2010 Jul 26
	H	WIRC	20.66±0.38	30	2	15	900	2010 Jul 26
WISEP J1828+2650	J	NIRC2	23.57±0.35	120	1	6	720	2010 Jul 01
	H	NIRC2	22.85±0.24	120	1	9	1080	2010 Jul 01
WISEPC J2056+1459	J	WIRC	19.31±0.12	60	1	15	900	2010 Aug 29
	H	WIRC	>19.5	30	2	15	900	2010 Aug 29
	J	NIRC2	19.21±0.07	120	1	9	1080	2010 Jul 01
	H	NIRC2	19.56±0.18	120	1	6	720	2010 Jul 01

TABLE 3
Spectroscopy Log

Object	Instrument	UT Date	Mode	Slit Width (arcsec)	Int. Time (sec)	A0 V Calibrator Star
WISEPC J0148−7202	FIRE/Magellan	2010 Sep 18	Longslit	0.6	960	HD 1881
WISEP J0410+1502	FIRE/Magellan	2010 Nov 18	Longslit	1.0	600	HD 18620
UGPS 0722−05	SpeX/IRTF	2011 Jan 26	LowRes15	0.5	1440	HD 50931
WISEP J1405+5534	WFC3/HST	2011 Mar 14	G141	⋯	2212	⋯
WISEP J1541−2250	FIRE/Magellan	2011 Mar 27	Longslit	0.6	1522	HD 130755
WISEP J1738+2732	WFC3/HST	2011 May 12	G141	⋯	2012	⋯
WISEP J1828+2650	WFC3/HST	2011 May 09	G141	⋯	2012	⋯
WISEPC J2056+1459	NIRSPEC/Keck	2010 Oct 21	low-res (N3)	0.38	2400	HD 198070
	NIRSPEC/Keck	2010 Nov 22	low-res (N5)	0.38	1800	HD 198069

TABLE 4
Spectral Indices

Object	Spectral Type	H$_2$O$-J$	CH$_4-J$	H$_2$O$-H$	CH$_4-H$	W$_J$	NH$_3-H$
UGPS 0722$-$05[a]	T9	$+0.009$ (0.004)	$+0.115$ (0.003)	$+0.115$ (0.007)	$+0.075$ (0.005)	$+0.215$ (0.003)	$+0.527$ (0.008)
WISEPC J0148$-$7202	T9.5	-0.017 (0.011)	$+0.076$ (0.006)	$+0.070$ (0.013)	$+0.016$ (0.012)	$+0.152$ (0.006)	$+0.431$ (0.015)
WISEP J0410+1502	Y0	-0.043 (0.090)	$+0.036$ (0.059)	-0.036 (0.458)	-0.105 (0.434)	$+0.155$ (0.052)	$+0.380$ (0.574)
WISEPC J1405+5534	Y0 (pec?)	$+0.020$ (0.026)	$+0.031$ (0.017)	$+0.063$ (0.025)	$+0.162$ (0.028)	$+0.099$ (0.017)	$+0.346$ (0.027)
WISEP J1541$-$2250	Y0	-0.046 (0.115)	$+0.040$ (0.060)	$+0.155$ (0.216)	$+0.057$ (0.208)	$+0.081$ (0.066)	$+0.259$ (0.200)
WISEP J1738+2732	Y0	$+0.036$ (0.008)	$+0.050$ (0.005)	$+0.045$ (0.008)	$+0.050$ (0.009)	$+0.149$ (0.005)	$+0.349$ (0.010)
WISEP J1828+2650	$>$Y0	$+0.248$ (0.152)	$+0.257$ (0.099)	$+0.049$ (0.091)	$+0.129$ (0.101)	$+0.515$ (0.106)	$+0.503$ (0.110)
WISEPC J2056+1459	Y0	$\cdots$	$+0.030$ (0.009)	$\cdots$	$+0.050$ (0.034)	$+0.129$ (0.012)	$+0.240$ (0.031)

NOTE. — The H$_2$O$-J$ and H$_2$O$-H$ indices cannot be computed for WISEPC J205628.90+145953.3 because its spectrum does not span the entire wavelength range of the indices.
[a] The values differ from that measured by Lucas et al. (2010). Our two spectra agree well except deep in the CH$_4$ and H$_2$O absorption bands, where our spectrum exhibits lower flux levels. The reason for this discrepancy is unclear but it may be a result of the fact that the Lucas et al. spectrum was created by merging separate spectra that were absolutely flux calibrated using near-infrared photometry.

TABLE 5
Previously Published Brown Dwarfs with Spectral Types Later than T8

Object	Previous Spectral Type	Reference	Adopted Spectral Type
Ross 458C	T8	Burgasser et al. (2010)	T8
	T8.5p	Burningham et al. (2011a)	$\cdots$
ULAS J123828.51+095351.3	T8.5	Burningham et al. (2008)	T8
ULAS J130217.21+130851.2	T8.5	Burningham et al. (2010)	T8
ULAS J003402.77$-$005206.7	T8.5	Warren et al. (2007)	T8.5
	T9	Burningham et al. (2008)	$\cdots$
CFBDS J005910.90$-$011401.3	$\gtrsim$T9	Delorme et al. (2008)	T8.5
	T9	Burningham et al. (2008)	$\cdots$
WISEPC J045853.90+643451.9	T9	Mainzer et al. (2011)	T8.5
UGPS J052127.27+364048.6	T8.5	Burningham et al. (2011b)	T8.5
ULAS J133553.45+113005.2	T9	Burningham et al. (2008)	T8.5
Wolf 940B	T8.5	Burningham et al. (2009)	T8.5
WISEPC J181210.85+272144.3	T8.5:	Burgasser et al. (2011)	T8.5:
UGPS J072227.51$-$054031.2	T10	Lucas et al. (2010)	T9
CFBDSIR J145829+101343AB	T9.5	Liu et al. (2011)	T9

TABLE 6
Atmospheric and Structural Properties

Object	SpType	$T_{\rm eff}$ (K)	$\log g$ (cm s^{-2})	$\log K_{\rm zz}$ (cm^2 s^{-1})	R ($R_{\rm Jup}$)	M ($M_{\rm Jup}$)
UGPS 0722$-$05	T9	650	4.00 (4.00$-$4.25)	4	1.21 (1.14$-$1.21)	6 (6$-$9)
WISEPC J0148$-$7202	T9.5	500 (500$-$500)	4.50 (4.50$-$4.75)	4	1.04 (0.96$-$1.04)	13 (13$-$21)
WISEP J0410+1502	Y0	450 (400$-$500)	3.75 (3.75$-$4.25)	0	1.22 (1.09$-$1.22)	3 (3$-$9)
WISEPC J1405+5534	Y0 (pec?)	350	5.00	4	0.86	30
WISEP J1541$-$2250	Y0	350	4.50 (4.25$-$4.5)	4	1.01 (1.01$-$1.07)	12 (8$-$12)
WISEP J1738+2732	Y0	350 (350$-$400)	4.75 (4.75$-$5.00)	4	0.93 (0.86$-$0.94)	20 (20$-$30)
WISEP J1828+2650	$>$Y0	$\leq$300	$\cdots$	$\cdots$	$\cdots$	$\cdots$
WISEPC J2056+1459	Y0	350 (350$-$400)	4.75 (4.50$-$5.00)	4	0.93 (0.86$-$1.01)	20 (12$-$30)

NOTE. — The parameters for the best fitting Marley & Saumon models are listed and the range of parameters consistent with the data is given in parentheses. The effective temperature limit for WISEP J1828+2650 was estimated by identifying those models with peak J-band fluxes equal to or less than the peak flux in the H band and by comparing the observed $J-$W2 color to model $J-$W2 colors.

TABLE 7
DISTANCE ESTIMATES

Object	SpType	d_{spec} (pc)[a]	d_π (pc)[b]	d_{phot} (pc) [c]
UGPS 0722−05	T9	11.1 (10.4−11.1)	3.6−4.7	⋯
WISEPC J0148−7202	T9.5	14.7 (13.1−14.7)	⋯	12.1
WISEP J0410+1502	Y0	7.1 (3.3−8.7)	⋯	9.0
WISEPC J1405+5534	Y0 (pec?)	3.8	⋯	8.6
WISEP J1541−2250	Y0	1.8 (1.8−2.0)	2.2−4.1	8.2
WISEP J1738+2732	Y0	3.4 (3.4−7.3)	⋯	10.5
WISEP J1828+2650	>Y0	⋯	⋯	<9.4
WISEPC J2056+1459	Y0	3.0 (2.4−6.4)	⋯	7.7

[a] Spectroscopic distance estimates derived as described in §4.2.1. The distance corresponding to the best fitting model is given and the range of distances corresponding to models that are consistent with the data are given in parentheses.
[b] Parallactic distance for UGPS 0722−05 and WISEP J1541−2250 from Lucas et al. (2010) and Kirkpatrick et al. (2011), respectively.
[c] Photometric distance estimates from Kirkpatrick et al. (2011).